# IN-SITU OBSERVATION OF EXTRUSION PROCESS IN THERMOPLASTIC MATERIAL EXTRUSION-BASED ADDITIVE MANUFACTURING

by

YE HONG

DISSERTATION

Submitted in partial fulfillment of the requirements
for the degree of Doctor of Philosophy at
The University of Texas at Arlington

August 2022

Arlington, Texas

Supervising Committee:

Cheng Luo, Supervising Professor
Xinchuan Liu
Ankur Jain
Yi Hong
Md Rassel Raihan

ACKNOWLEDGEMENTS

I thank Dr. Cheng Luo my supervising professor for his guidance, and helpful discussion throughout this research work.

I thank Dr. Xinchuan Liu of Virginia State University for his time and effort in benchmarking the numerical simulation section.

I thank my Supervising Committee members for their valuable suggestions and all the help they offered.

I would like to acknowledge Dr. Manjarik Mrinal, Dr. Kathy Hays-Stang, Dr. Amirhossein Mostafavi, and Parimal Patel for helpful discussions regarding various aspects of this work. Acknowledgement also extends to my academic advisers who guided me in this process.

# DEDICATION

I dedicate my dissertation work to my family. Gratitude to my parents, Hong Huiqun and Yang An, for their words of encouragement and push for tenacity kept me going. The presence of my little cousins Yang Wenlan, and Liang Luwei during this difficult pandemic time is very special.

I dedicate my dissertation work to Songwei Wang and Manjarik Mrinal for their friendship.

I dedicate my dissertation work to Dr. Cheng Luo for sharing his personal view and insight on research work in general.

LIST OF FIGURES

LIST OF TABLES

# LIST OF ABBREVIATIONS

| | |
|---|---|
| *AM* | Additive Manufacturing |
| *SLA* | Stereolithography |
| *SLS* | Selective Laser Sintering |
| *SLM* | Selective Laser Melting |
| *DMLM* | Direct Metal Laser Melting |
| *MatEx* | Material Extrusion |
| *FDM* | Fused Deposition Modeling |
| *FFF* | Fused Filament Fabrication |
| *GNF* | Generalized Newtonian Fluid |
| *ABS* | Acrylonitrile Butadiene Styrene |
| *PLA* | Polylactic Acid |
| *WLF* | Williams–Landel–Ferry |

NOMENCLATURES

| | | |
|---|---|---|
| $U$ | *mm/s* | Filament feed rate |
| $U_M$ | *mm/s* | Modified filament feed rate |
| $V$ | *mm/s* | Measured flow speed at center of flow |
| $T$ | *°C or K* | Temperature |
| $T_e$ | *°C or K* | Extrusion temperature |
| $T_r$ | *°C or K* | Reference temperature |
| $T_g$ | *°C or K* | Glass transition temperature |
| $T_i$ | *°C or K* | Interface temperature |
| $T_c$ | *°C or K* | Critical temperature |
| $\rho$ | $g/cm^3$ | Density |
| $C_P$ | *J/kg-K* | Specific heat capacity |
| $k$ | *W/m-K* | Thermal conductivity |
| $k_{eff}$ | *W/m-K* | Effective thermal conductivity |
| $h$ | $W/m^2$*-K* | Heat convection coefficient |
| $\eta$ | *Pa.s* | Viscosity |
| $\eta_r$ | *Pa.s* | Consistency index at reference temperature |
| $n$ | - | Power-law index |
| $C_1$ | - | Williams-Landel-Ferry constant 1 |
| $C_2$ | *°C or K* | Williams-Landel-Ferry constant 2 |
| $\alpha_T$ | - | Horizontal shift factor |

| | | |
|---|---|---|
| $E_a$ | *J/mol-K* | Activation Energy |
| $\alpha$ | $m^2/s$ | Thermal diffusivity |
| $L_h$ | *mm* | Tube length, straight section |
| $L_c$ | *mm* | Tube length, conical cone section |
| $L_n$ | *mm* | Tube length, nozzle section |
| $L_m$ | *mm* | Temperature/Speed measurement location |
| $d$ | *mm* | Diameter, filament |
| $d_n$ | *mm* | Diameter, nozzle |
| $d_t$ | *mm* | Diameter, tube outer |
| $d_i$ | *mm* | Diameter, tube inner |
| $\Delta t$ | *s* | Time interval in video image analysis |

ABSTRACT

# In-situ Observation of Extrusion Process in Thermoplastic Material Extrusion-Based Additive Manufacturing

Ye Hong, Ph.D.

The University of Texas at Arlington, 2022

Supervising Professor: Cheng Luo

In thermoplastic material extrusion based additive manufacturing, solid polymer filaments are fed into extruders to generate extrudates that are needed to build 3D plastic products. There is a finite gap between the inner surface of an extruder and the edge of a filament. This gap facilitates the insertion and translation of the filament inside the extruder. However, it is still not clear how the gap is filled during the extrusion. The lack of this information makes it difficult to model the temperature distribution and flow profile during the extrusion. In this work, we built experimental apparatus to directly observe the gap-filling processes of Acrylonitrile Butadiene Styrene (ABS) and Polylactic Acid (PLA) filaments, for different combinations of extrusion temperatures and feed rates. Although ABS and PLA are, respectively, amorphous and semi-crystalline polymers, for both materials, we found: i) the gap inside an extruder was filled through three different steps during the initial stage of extrusion; ii) the gap-filling level depended on extrusion temperature and feed rate; and iii) there was no noticeable difference in the gap-filling level when the extrusion started with an empty tube or resumed after the printing had been paused. The steady extrusion

processes of ABS were simulated with computational fluid dynamic software. Two sets of simulations were conducted: one with a glass tube and the other with an aluminum tube. The numerical results for the case of glass tube were validated by comparing them with experimental results. The simulation results indicated: 1) when polymer flow was sufficiently heated, the flow characteristics were similar in the cases of glass and aluminum tubes; 2) if the feed rates were high, due to shorting heating time and low thermal diffusivity of the polymeric material, the polymer were insufficiently heated and clogging might occur; and 3) as the heat transferred faster through the aluminum tube to the polymer, the feed rate that caused clogging in the case of the aluminum tube was higher than its counterpart in the case of the glass tube.

TABLE OF CONTENTS

# CHAPTER 1

# INTRODUCTION

## 1.1. 3D Printing in a Brief

The additive manufacturing (AM) method in the form of 3D printing we know today began to take shape in the 1980s. In the early 1980s, Hideo Kodama of Nagoya Municipal Industrial Research Institute filed a patent [1] and presented research resulting in publication [2] for a three-dimensional building device using liquid photo-hardening polymer, which became the early version of the Stereolithography (SLA) type 3D printer. Later in 1984, Alain Le Méhauté, Olivier de Witte, and Jean Claude André filed their patent on the SLA device in France [3]. However, both projects were abandoned due to the lack of interest at the time. In the same year, Charles Hull filed a patent for developing an apparatus that generates three-dimensional objects by curing photosensitive resin layer-by-layer with UV light [4].

In 1986, Dr. Carl Deckard of the University of Texas at Austin first patented the selective laser sintering (SLS) technology, which fuses polymeric material in powder form with a laser [5]. A few years later, similar to the laser based SLS process selective laser melting (SLM), also known as direct metal laser melting (DMLM), was developed by Fraunhofer Institute ILT in Aachen, Germany [6], making additive manufacturing with metal possible by using a high-power laser to melt and fuse metallic material in powder form.

In 1989, Scott Crump patented the additive manufacturing method known as material extrusion (MatEx), fused deposition modeling (FDM), or fused filament fabrication (FFF) [7].

Different from the SLA and SLS type machine's light source-based technologies, the MatEx machine extrudes polymer filament directly through the heated extruder and deposits the extrudate on the heated building stage layer by layer.

With the maturation of these technologies in the following decades, other advancement in variants of printing technologies, and improvement in computer aid design (CAD), together they form today's 3D printing industry. In the present day, the 3D printing device can produce objects with greatly improved quality at a fraction of the cost, at the same time, offer numerous customization options, rapid production, and unique mechanical properties. It is for these reasons 3D printing technology has gained interdisciplinary interests from industries such as medical, automotive, civil, etc.

## 1.2. Statement of Purpose

Although the MatEx type of 3D printing is by far the most accessible by public due to its ability of producing cost-effective parts in a rapid manor, the exact process of polymer extrusion remains uncertain. The core interest of this work is to gain fundamental understanding of the polymer flow behavior within the heated extruder in both transient and steady condition. The extrusion process in MatEx type of 3D printers is systematically studied with qualitative in-situ observations. Then, the extrusion process is generalized by using numerical simulation works. There are two purposes of this work: first, to provide a clear understanding of the polymer extrusion process in various scenarios during common use; second, the numerical simulation of

the extrusion process can provide information which is considered hard to obtain from experimental work.

## 1.3. Significance of the Study

The in-situ observation reveals the extrusion process for MatEx type of 3D printers. The observations address the core interest of polymer flow development inside extruder in both transient and steady extrusion conditions, in the meantime provided visual reference for numerical simulation. The associated flow profile and temperature distribution inside extruder in steady extrusion conditions are obtained through numerical simulation. The simulated results were validated with the measured flow magnitude. Additional numerical simulation work of extrusion in metal tube were attempted to generalize the findings. This series of work is significant towards optimizing the printing parameters in the MatEx process.

## 1.4. Overview

The layout of the rest of the dissertation is as follows: Chapter 2 presents the literature review of recent related work done by other scholars. In Chapter 3, the structure of this research work is introduced at the beginning of the chapter, following with the detailed presentation of the experimental apparatus and test materials. This chapter presents the in-situ observation part of the work, several criterions of tests, limitations of the experimental apparatus, as well as the validation of gap-filling theory are explained, justified, and presented, respectively. This chapter ends with

the numerical model, including the governing equations, the geometry, the boundary conditions, and the treatment of the material properties are also presented in this chapter. Chapter 4 presents and discusses the results from both the in-situ observation and numerical simulation. The work is summarized, the findings are listed, and the conclusions are made in Chapter 5.

# CHAPTER 2

# LITERATURE REVIEW

MatEx, also known as fused-deposition modelling or fused-filament fabrication, is one of the most widely used processes to print 3D plastic structures [8, 9]. In MatEx, a solid polymer filament is fed into a heated tube, and it melts while traveling down the tube. The polymer melt that is extruded from the tube is deposited on a build plate layer by layer to form a desired 3D product. There is a finite gap ($\approx$ 0.13 mm) between the edge of the filament and the inner surface of the heated tube, which facilitates its insertion and translation [8]. It leads to extra thermal resistance to heat transfer from wall to filament. After the polymer travels a certain distance inside the tube, it may be molten. The polymer melt may then fill the gap [8]. For the portion of the tube, which ranges from the entrance to the location where the polymer gets molten, the gap is proposed to be filled by backflow of the polymer melt [10, 11]. This proposed filling mechanism was simulated in Serdeczny et al's analysis [12].

To find optimal process parameters for MatEx, several analytical models have been developed to determine the distributions of temperature [13, 14, 15, 16, 17] and pressure [14, 17] inside extruders. These models were developed based on traditional thermal [18, 19, 20, 21, 22, 23] and pressure [24] models used in plastic manufacturing. These traditional models focus on polymer melt flows in tubes, with the tubes fully filled by polymer melts. Accordingly, in the MatEx models [13, 14, 15, 16, 17], the gap in a tube was also assumed to be fully filled by the polymer.

On the other hand, to our knowledge, there is no direct observation regarding how the gap is filled and how much of the tube is filled. As a matter of fact, such observation is important to validate the proposed gap-filling models [8, 10, 11, 12] and the "fully-filled" assumption made in the theoretical models [13, 14, 15, 16, 17]. It is also helpful for choosing process parameters, such as extrusion temperature and feed rate, in printing a 3D part. Therefore, in this work, we conduct in-situ observation of the processes that ABS and PLA are extruded inside heated glass tubes. Both ABS and PLA are polymers commonly used in MatEx additive manufacturing [8, 9, 10, 11, 12, 13, 14, 15, 16, 17], [25], [26]. ABS is an amorphous polymer, while PLA is a semi-crystalline one.

Analytical, experimental, and numerical studies from various approaches were carried out on polymer flow inside the extruder, as well as after the formation of extrudate on the build plate. Luo et al. [27] classified deposited extrudate's bonding width characteristics in terms of printing parameters of nozzle height and nozzle speed. A rapid screening process for extrudability done by Gilmer et al [10], where they considered the extrudability in two failure modes: annular backflow and filament buckling inside the extruder hot-end. An analytical model proposed by Osswald et al. [28] for a limited case scenario for the maximum melting rate is controlled by the extrusion force. In this case, the polymer melt zone within the extruder hot-end is reduced to a melt film only at the tip of the filament. In the experimental and analytical study by Serdeczny et al. [25] on the polymer flow inside extruder hot-end, they identified the stable and unstable extrusion regime by measuring the feed force. Then, they proposed a heat transfer model to estimate the maximum feed rate of stable extrusion regime. Luo et al. [16] proposed an analytical model of predicting the upper bond feed rates by assuming that the maximum feed rate occurs when the solid tip of filament blocks the nozzle exit entirely while neglecting the gap between

solid filament and the tube inner wall. The analytical prediction of upper bond feed rate shows good agreement with the experimental result. Peng et al. [29]visualized the polymer flow inside the extruder hot-end by inserting pigment in different color. They concluded that the extrusion process is non-isothermal, especially in high extrusion speed case.

Computational fluid dynamics (CFD) simulation of the polymer flow inside the extruder was attempted by Serdeczny et al. [12]. From the polymer enters the extruder hot-end till extrusion reached steady state with two models. One used one-phase model with fully filled simulation domain; while in the second model, they modeled the free surface of the polymer inside the channel at the upper end of the heated zone. The molten ABS polymer was simulated as a Generalized Newtonian Fluid (GNF) with shear- and temperature dependent viscosity. The thermal resistance at the channel's wall was estimated by experimenting with different heat transfer coefficients. Small recirculation region was also captured in the second simulation model. Phan et al. [30] simulated the polymer melting process in fused filament fabrication (FFF) additive manufacturing using GNF model. They found that almost half the pressure drop occurred over the conical nozzle region where polymer flow converges.

# CHAPTER 3

# METHODOLOGY

## 3.1. Study Design

The study plan of this research work consists of both experimental and numerical work (Figure 1). In the work, an experimental apparatus which closely resembles a common extruder of commercial MatEx 3D printer is built for in-situ observation purposes. Then, criterion of determining the gap-filling condition is developed using light deflection theory. The extrusion process using experimental apparatus is validated with the commercially available extruder. The extrusion processes are then observed in two categories: the transient extrusion and the steady extrusion. In transient extrusion by observing the extrusion processes in three common scenarios - including extrusion from initially empty tube, extrusion during material changes, as well as resume extrusion after cool-down - a gap-filling model was determined. In steady extrusion, the polymer flow development in terms of feed rate is investigated, and the flow profiles are measured for the comparative purpose with the numerical work.

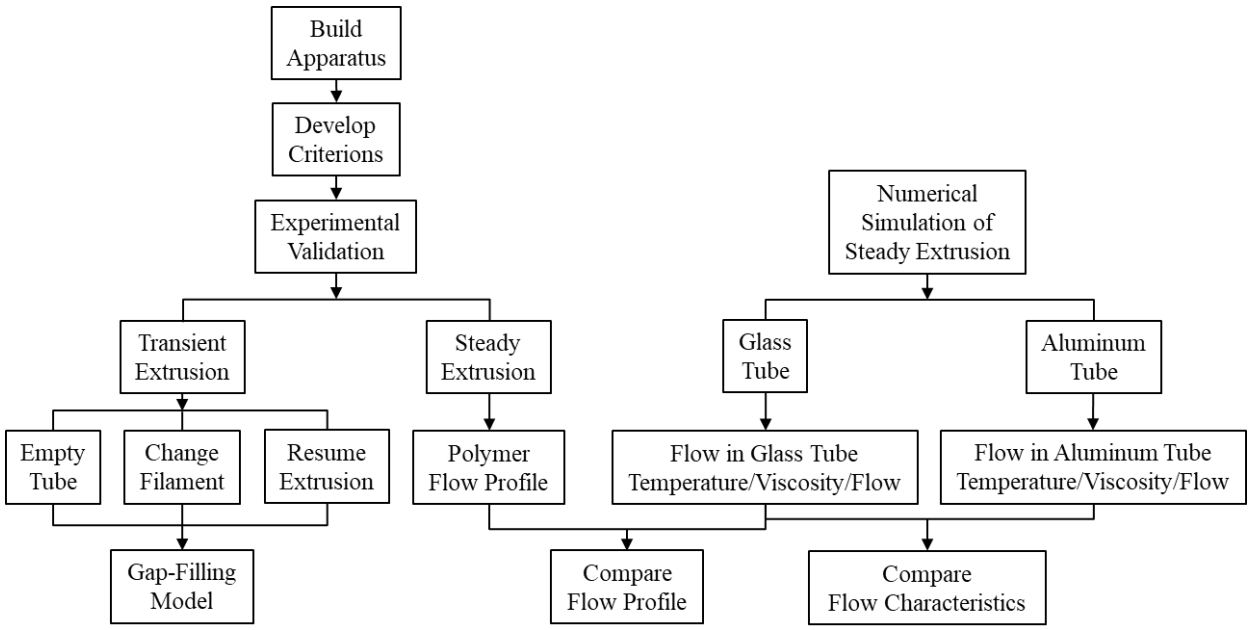


*Figure 1. Study design plan*

In the numerical work, the simulation model and boundary conditions are based on the dimension of experimental apparatus and operating conditions, respectively. The intent of the numerical work is to explore and investigate the difference between the experimental apparatus and the commercially available extruder. The steady extrusions are simulated using both glass tube and aluminum tube in same dimension and boundary conditions. From the glass tube cases, the simulated flow profiles are compared to the experimentally observed ones. The flow profile comparison not only helps validate numerical method used in the simulation, but also resolves the temperature distribution and local viscosity of the flow. The flow characteristic comparisons are then carried out between glass tube cases and aluminum tube cases, which address the tube material concern in the experimental apparatus and validate the numerical method for generation purpose.

## 3.2. Experimental Setup for In-situ Observation

### *3.2.1. Experimental Apparatus*

We built an experimental apparatus to closely resemble a typical extruder used in a MatEx 3D printer. It included a driving system, a fan, a borosilicate glass tube (Chang Bioscience, Fremont, CA, USA), an observation chamber, and a heat-supply system (Figure 2). Table 1 lists the dimensions of the observation chamber and glass tube, as well as the operational ranges of feed rates ($U$) and extrusion temperature ($T_e$).

For observation purposes, the metal extruder in MatEx printer were replaced by the transparent glass tube and heated chamber, respectively. The glass tube consists of a cylindrical session and a conical nozzle (Figure 2). The exit of the conical nozzle was measured at 0.4 mm in diameter. The cylindrical session had a uniform cross-section with an inner diameter in the range of 2.04 – 2.09 mm. Its wall was measured about 1 mm thick. The lower portion of the glass tube with a length of 3 cm was inserted into the observation chamber, and it was heated during an extrusion. The upper portion of the glass tube, which also has a length of 3 cm, was exposed above the chamber. During an extrusion, it was cooled by the fan located beside it.

The front and back sides of the chamber were glass plates, which were used to observe an extrusion process that occurs inside a glass tube. The glass tube was located in the center of the chamber. The heat-supply system consists of an air pump, a hot plate, and a heat exchanger. The heat exchanger was heated by the hot plate underneath. Air was supplied to the heater exchanger by the air pump. The air was first heated up in the heat exchanger, and then flowed into the observation chamber at a constant rate to provide the heat needed for an extrusion process. The air flow speed was measured at 0.4 – 0.5 m/s, equivalent of volume flow rate of $2.3\times10^{-5}$ – $2.8\times10^{-}$

$^{5}$ $m^3/s$, which were measured using an anemometer (BTMETER BT-100, China). The dotted box in Figure 2 marks the area of interest for observation. Extrusion processes were recorded using a digital microscope (Dino-Lite Pro, Torrance, CA, USA).

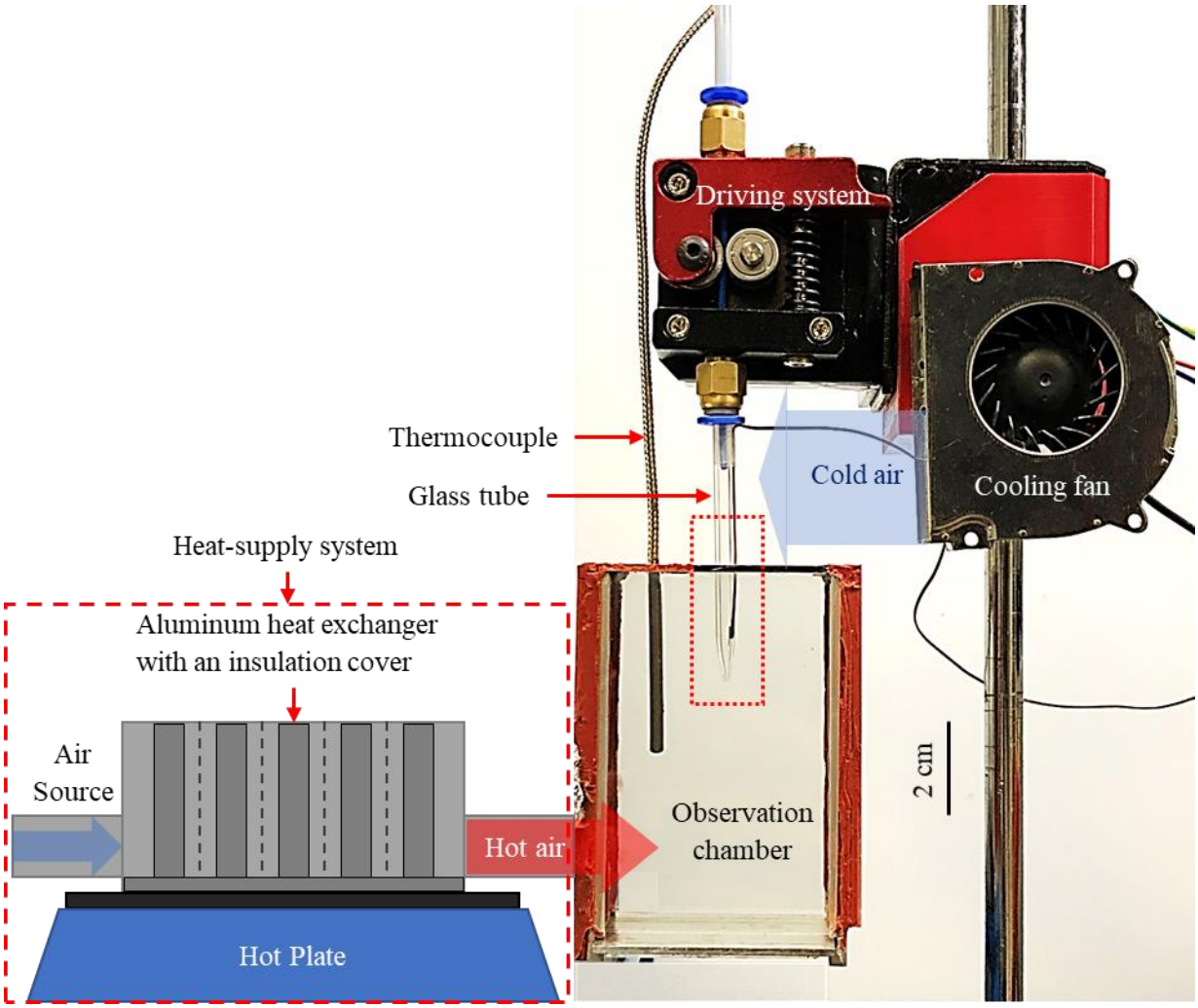


*Figure 2. Experimental setup for in-situ observation. The dashed dox marks the heat-supply system, and the dotted box indicates the area of interest for observing the extrusion.*

The driving system includes a stepper motor (NEMA 17, Shenzhen, China), a microcontroller, a programmable microcontroller (Arduino UNO R3, Turin, Italy), a motor driver

(TB6600, Shenzhen, China), and two gears. The filament feed rate at the stepper motor was digitally controlled by the microcontroller via the motor driver. The feed rate calibration curve and control program are provided in APPENDIX I.

*Table 1. Dimensions and constants of the experimental apparatus*

| Dimension | Units | Value Range (error) | Measurement Accuracy |
|---|---|---|---|
| Chamber height | *cm* | 10.0 | 0.1 |
| Chamber width | *cm* | 2.5 | 0.1 |
| Chamber length | *cm* | 5.0 | 0.1 |
| Length of glass tube's heated portion | *cm* | 3.0 | 0.1 |
| Length of glass tube's cooled portion | *cm* | 4.0 | 0.1 |
| Thickness of tube wall | *mm* | 0.98 - 1.02 | 0.01 |
| Inner diameter of glass Tube's inner diameter | *mm* | 2.04 - 2.09 | 0.01 |
| Length of conical nozzle | *mm* | 0.5 - 0.7 | 0.1 |
| Diameter of nozzle's exit | *mm* | 0.4 | 0.01 |
| Filament feed rate ($U$) | *mm/s* | 0.2 - 7.0 | 0.1 |
| Extrusion temperature ($T_e$) | *°C* | 20 - 240 | 0.4 |

The temperature inside the chamber was measured using K-Type thermocouples (OMEGA Engineering, Norwalk, CT, USA) at multiple locations with the aid of a data acquisition system (National Instrument 9212 C series & LabVIEW, Austin, TX, USA). This temperature was controlled with an error of 5 °C by adjusting the power level of the hot plate. It was also the setting

temperature for an extrusion process. The block diagram for temperature monitoring and recording is provided in APPENDIX II.

*3.2.2. Test Materials*

Acrylonitrile Butadiene Styrene (ABS) [31] and Polylactic Acid (PLA) [32] filaments with different colors were adopted for our tests. We tested ABS filaments in transparent blue, transparent orange and solid white colors, and PLA filaments in transparent yellow, and solid red colors. The filaments' dimensions and manufacturer suggested extrusion temperature ranges are listed in Table 2.

*Table 2. Material properties of tested ABS and PLA filaments*

| | Units | Blue & Orange ABS | White ABS | Yellow PLA | Red PLA |
|---|---|---|---|---|---|
| Manufacturer | - | HATCHBOX [31, 32] | | | |
| Diameter of the filament ($d$) | *mm* | 1.75 ± 0.05 | 1.75 ± 0.03 | 1.75 ± 0.03 | 1.75 ± 0.05 |
| Extrusion temperature ($T_e$) | *°C* | 210 – 240 | 210 – 240 | 180 – 210 | 180 – 210 |
| Melting Temperature ($T_m$) | *°C* | - | - | 155 | 155 |
| Density ($\rho$) | $g/cm^3$ | 1.20 (measured) | 1.19 (measured) | 1.27 | 1.27 |

As shown in the same kind of material, there was little difference between transparent and solid color filaments in the listed specification. Moreover, during the tests, there did not show distinctive differences in their performance of the same kind. Both the ABS and PLA filaments have the same mean diameter of 1.75 mm. When they were inserted into glass tubes, the gap was about 0.15 mm wide between the edge of a filament and the inner surface of a glass tube.

Both ABS and PLA require drying prior testing and both filaments were baked in the oven to remove moisture at 80 °C and 50 °C for at least 4 hours prior testing, respectively.

### *3.2.3. Material Preparation*

Two types of 3-color filament were custom-made out of the three colored ABS filaments, to visualize the polymer flow during the extrusion. For the transient extrusion case-studies (Figure 3(a)), the orange and blue sections were both 1 cm long. The trailing white section had a length of at least 15 cm, to ensure that the filament was long enough to run through the glass tube. The shown example in Figure 3(b), the orange and blue section were both 6-cm-long, with a long trailing white section (> 15 cm) for the case-studies of steady extrusion of $U$ = 1 mm/s case. Note that the length of the first section (Orange) needs to be sufficiently long to reach steady extrusion. The length of the second section (Blue) had less restriction since the observations were focused on the changing boundary shape between the first and second section. These sections were bonded at their interfaces with a cement (TAMIYA 87038, Shizuoka, Japan), which contained acetone and butyl acetate. In addition, solid color filaments were applied to determine the three gap-filling regions, which will be shown in Figure 11.

The jointing method used for ABS filaments is ineffective for jointing the PLA. Therefore, only the 3-color ABS filaments were the ones that were used in all our tests to observe the flow patterns of polymer melts during an extrusion. The PLA filaments were applied to validate the observed phenomena.

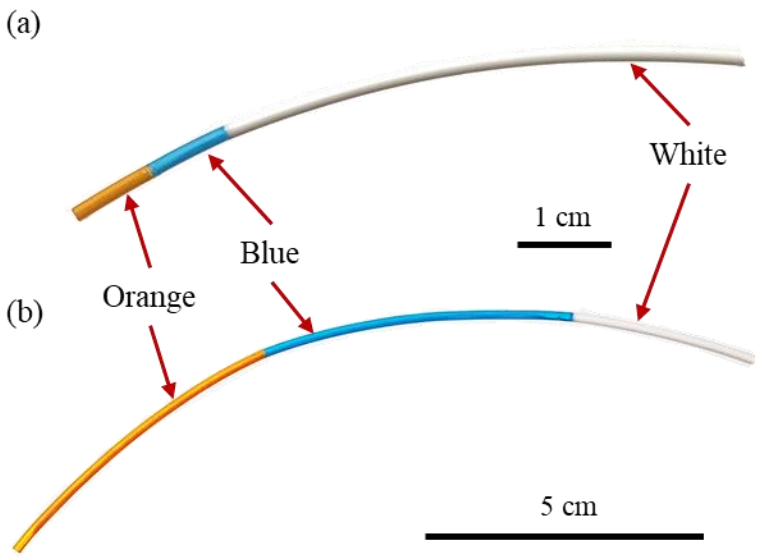


*Figure 3. Two types of 3-color ABS filament for in-situ observation.*

### *3.2.4. Test Procedures*

For both transient and steady state filament extrusion in-situ observation test, each test consists of five steps:

(1) All filament in the testing was subject to the same drying procedure listed in section 3.3.3.

(2) Set up the experimental apparatus as shown in Figure 2.

(3) Adjust the power level of the hot plate to control the temperature within the observation chamber.

(4) Program the microcontroller to control the feed rate.

(5) When the temperature reached desire extrusion temperature ($T_e$), then turn on the stepper motor, and observe the extrusion process.

*3.2.5. Criterion of Clogging*

Clogging inside the glass tube was determined according to gear slip in the driving system. A filament was driven into a glass tube as the gears rotated. In the event of clogging, since the resistance that the filament encountered inside the glass tube was larger than the driving force of the gears, the filament stopped to moving, while the gears were still rotating (Figure 4(a)). The rotating gears grinded off material from the filament, producing an abrasion mark on the filament (Figure 4(b)).

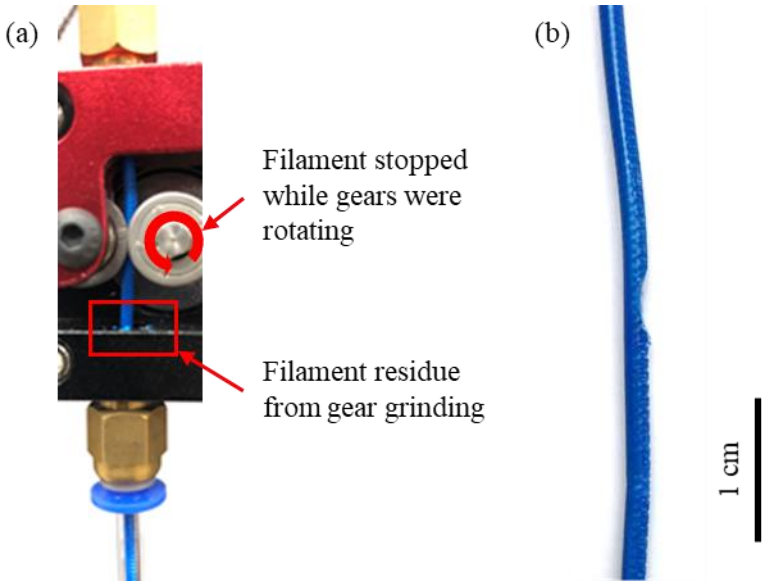


*Figure 4. Criterion of Clogging. (a) Clogged filament and grinded filament residue, and (b) a grinded ABS filament sample from a representative case of gear slip.*

The maximum feed force of our experimental setup was measured in terms of feed rate, using a precision universal tester (Shimadzu AGS-10kNXD, Kyoto, Japan) (Figure 5(a)). A filament was fed through the glass tube using the same driving system of our

experimental setup. The inverted "T" structure at the upper claw of the precision universal tester blocked the exit of the glass tube, making the filament clogged inside the tube. The measured maximum feed forces are plotted in terms of filament feed rate ($U$) Figure 5(b).

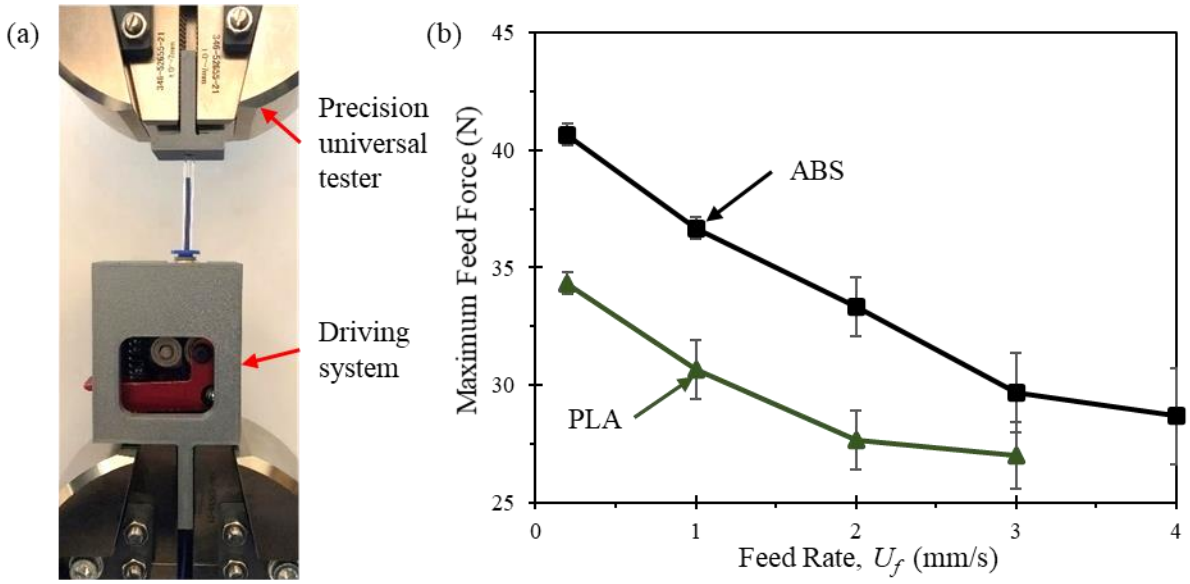


*Figure 5. Maximum feed force measurement. (a) measurement setup, and (b) relation of measured maximum feed force with feed rate. Error bar indicates the measuring error*

The measurement was performed at room temperature since temperature was not a factor of gear slip at the driving system. As shown in Figure 5(b), the measured maximum feed force decreased with the increase in feed rate. For example, the maximum force for feeding ABS decreased from 41 to 29 N as the feed rate increased from 0.2 to 4 mm/s. It was considered that when the feed rate was increased, more material was grinded off from the filament by the rotating gears. Consequently, the filament was easier to lose contact with the gears, leading to the decrease in the maximum feed force. As for ABS, the maximum feed forces used by other researchers are 35 N [16], 40 N [28], and up to 60 N

[12, 17], respectively. The maximum feed forces of ABS in our setup are comparable to these reported values. In the case of PLA, when the feed rate increased from 0.2 to 3 mm/s the maximum feed forces decreased from 34 to 26 N. They are comparable to the ones used in Serdeczny et al. [25], which was 30 N.

*3.2.5. Criterion of Gap-Filling Condition*

We utilized an optical effect of light refraction in a glass tube as the criterion to determine the gap-filling condition. In microfluidics, optical distortion of an object in a glass tube created difficulty in making accurate measurement of the object's dimensions. A correction method was used to solve this problem [33]. However, in our case, the optical distortion helped identify the gap-filling condition. As shown in Figure 6(a), when a blue ABS filament was inserted in a glass tube at room temperature, its image stayed inside that of the tube, with air gap visible between the filament and tube wall. For comparison, the bottom of the glass tube was pre-filled with ink. The image of the ink was wider than that of the filament. The two vertical lines marked in Figure 6(a) appeared to be the left and right edges of the tube wall. The image of the ink seemed to penetrate the tube wall. The boxed section of the tube was then heated by a blow torch (Bernzomatic, Columbus, OH, USA). The outer region of the contained filament should melt instantly. With a small force manually applied to push the filament, its image also appeared to penetrate inside the tube wall (Figure 6(b)). Since the images of the filament and ink had about the same lateral size, as in the case of ink, the filament should also have the full contact with the tube. After both the tube and filament were cooled down to room temperature, the filament contracted slightly, and its

image no longer penetrated the tube wall (Figure 6(c)). In contrast, the image of ink still appeared to be so. The same phenomena of the "penetration" were also observed when PLA filaments and white and orange ABS filaments were heated and slightly pressed. Accordingly, the appearance of penetration was used in this work to judge whether the gap around a particular portion of a filament was filled during the extrusion.

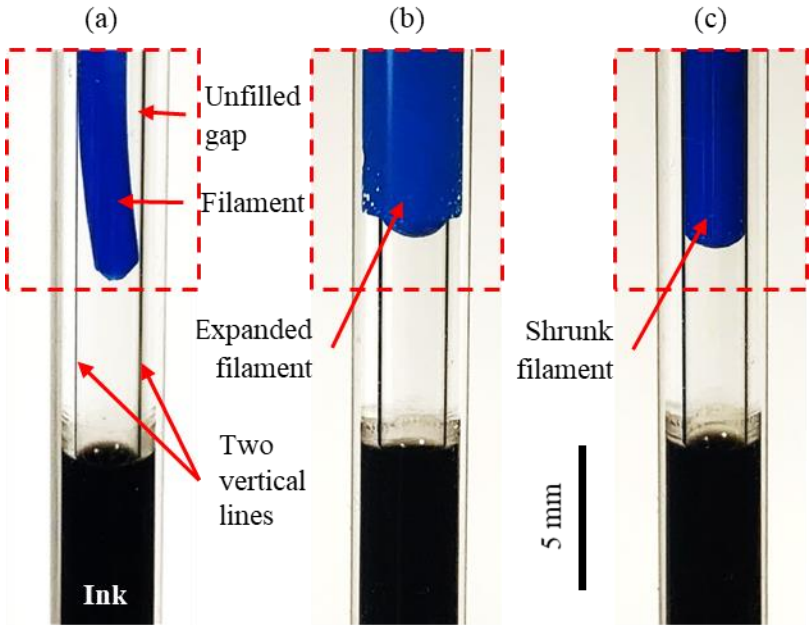


*Figure 6. Comparative images of filament with ink inside a glass tube. (a) filament at room temperature, (b) heated filament, and (c) cooled filament. All are side views.*

Consider the outer and inner surfaces of the glass tube as convex and concave lenses, respectively. The convex lens magnifies the image of an object, while the concave lens shrinks it. As such, the image of the filament in the case of Figure 6(a) was first shrunk by the inner surface of the tube and then enlarged by the outer surface of the tube. The same applied to the image of the filament in Figure 6(c). In the case of Figure 6(b), as there was no gap between the edge of

the filament and the inner surface of the tube, the image of the filament was just enlarged by the outer surface of the tube. As such, this filament, as well as the pre-filled ink, had an image wider than the filaments in (a and c) of Figure 6. A detailed explanation was given in [34] about a related optical distortion according to light ray paths, and also in APPENDIX III.

According to the testing result on a heated filament (Figure 6(b)), polymer melt could be driven to fill the gap around the filament. To determine the critical temperature ($T_c$), at or above which the polymer was soft enough to be driven around by a small feed force to fill the gap, the following experiment was conducted. A filament was fed into the tube at 0.2 mm/s, which was the lowest feed rate in our setting. This low feed rate ensured that the filament received enough heat as it moved down inside the tube. Since the feed rate was low, the corresponding feed force was also small. By gradually increasing the temperature within the observation chamber, $T_c$ was found to be 125 ± 5°C in the case of ABS. When the chamber temperature was at or above this temperature, the filament-insert fully filled the cross-section of the tube, as observed from its enlarged image. This critical temperature is higher than glass-transition temperature ($T_g$) of ABS, which is 105 °C [9]. Storage modulus of ABS drops sharply with temperature after the polymer reaches its $T_g$ [35]. Therefore, although the feed force was small, ABS still had a relatively large deformation at the measured $T_c$, to fill the gap around the filament.

As for PLA, $T_c$ was found to be 70 ± 5 °C. This value was about 10 °C higher than PLA's reported glass transition temperatures of 60 ± 5 °C [26] and 57.1 – 58.8 °C [36]. It is much lower than its reported melting temperatures of 155 °C [32] for our test material, or 160 – 170 °C [26] and 149 – 167.9 °C [36].

## 3.3. Validation and Application of Results to a Conventional MatEx Printer

### *3.3.1. Interface temperature measurement*

To have a good understanding about the temperature at the tube wall in our first setup (Figure 1), a thermocouple was used to measure the interface temperature, $T_i$ of filament and glass wall during steady-state extrusion. A 0.3-mm-diameter hole was drilled at the end of the straight portion of tube, which was about 0.7 cm above the nozzle exit. A 40 AWG K-type thermocouple was inserted into the hole for $T_i$ measurement (Figure 7(a)). The thermocouple was sealed and secured at the drilled hole with high temperature epoxy (J.B Weld 8297, Sulphur Springs, TX, USA), to prevent polymer leak from this location (Figure 7(a)).

For both ABS and PLA, $T_i$ drops with the increase in $U$ (Figure 7(b)). It was also lower than the corresponding $T_e$. Take the case of $T_e$ = 230 °C (ABS) as an example. At $U$ = 0.2, 1.0, 2.0, 3.0, or 4.0 mm/s, $T_i$ was 3, 8, 18, 35, or 47 °C lower than the corresponding $T_e$ (Figure 7(b1)). According to the relation of $T_i$ and $T_e$ (Figure 7(b)), the gap-filling results that were obtained in this study, such as Figure 15, may be used to approximately predict the result that would be obtained in a metal extruder with similar dimensions. An example was given as follows. According to Figure 7(b1), at $T_e$ = 230 °C and $U$ = 2.0 mm/s, it was a partial-filled case of ABS for our setup. In view of Figure 6(b), a similar gap-filling process may happen in the metal extruder, when the corresponding extrusion temperature was set to be $T_i$ = 218 °C with $U$ = 2.0 mm/s.

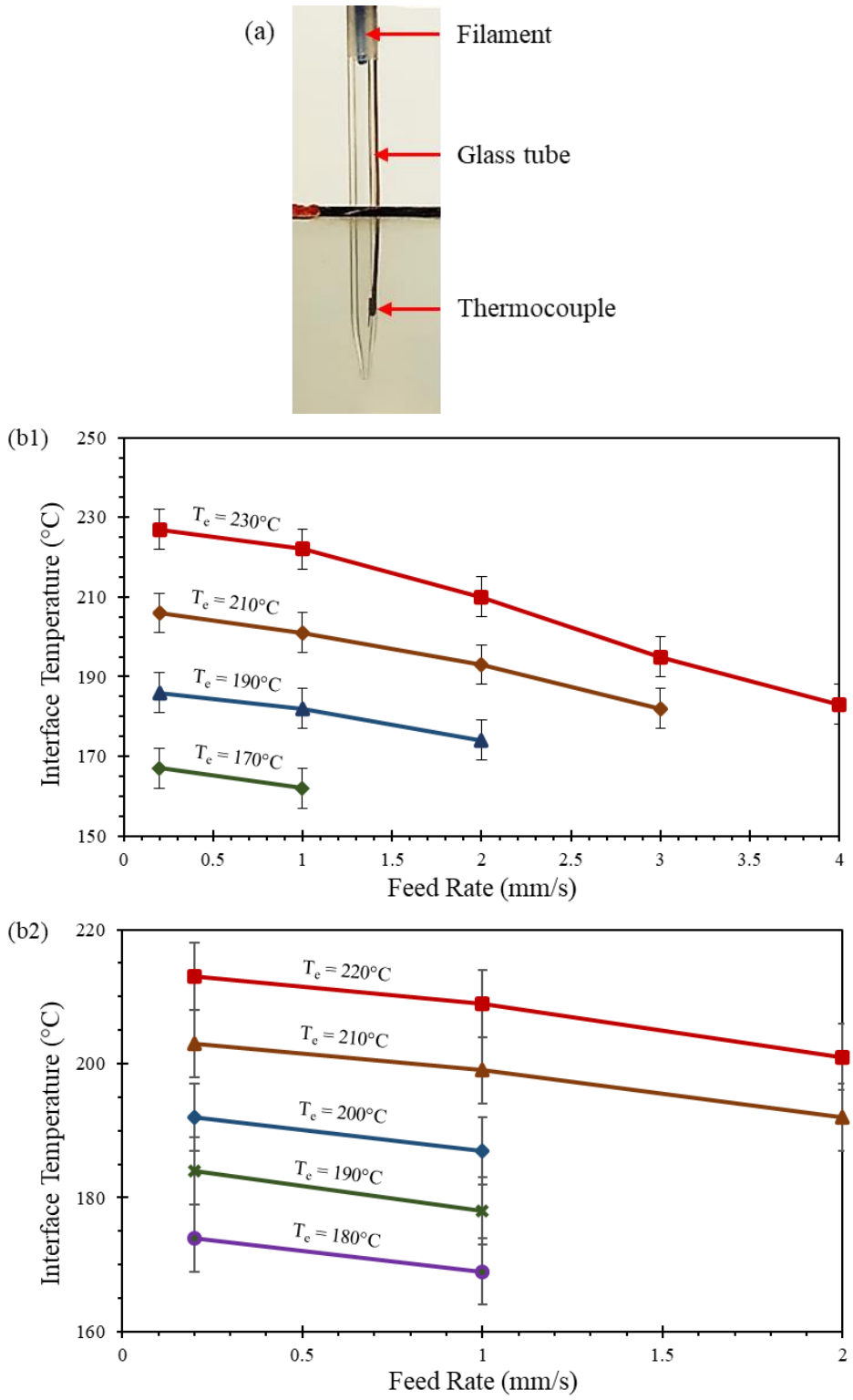


*Figure 7. Interface temperature measurement. (a) Measurement of the interface temperature $T_i$ at the end of the straight portion of the tube using a K-type thermocouple. (b) The relations of measured temperature with feed rate in the cases of ABS (b1) and of PLA (b2).*

*3.3.2. Benchmarking with Commercially Available 3D Printer*

In our setup, the heat was transferred from a hot environment, and the extruder was a glass tube. The hot environment had a temperature of the pre-set $T_e$. The heated tube initially also had a temperature of $T_e$. However, glass has a lower thermal diffusivity than a metal (Table 1). Heat was transferred slowly from the hot environment to the tube wall. Meanwhile, much heat was absorbed by a cold filament from the tube wall. Therefore, the tube wall may have a temperature lower than the pre-set $T_e$.

To validate the gap-filling process presented in Section 4.1 and illustrated in Figure 11, the extrusion of ABS and PLA filaments in a commercial extruder were explored. As our filament driving system could control the feed rate with a precision of 0.1 mm/s, we opted not to use the driving system of the commercial MatEx printer (Model: Creality3D Ender 5 Pro of Creality Company in Shenzhen, China). We attached our driving system to the temperature control system of the MatEx printer. As shown in Figure 8(a) and illustrated in Figure 8(b), this commercial extruder had a similar configuration to our glass extruder, while its materials, heating mechanism, and heated portion were different from ours.

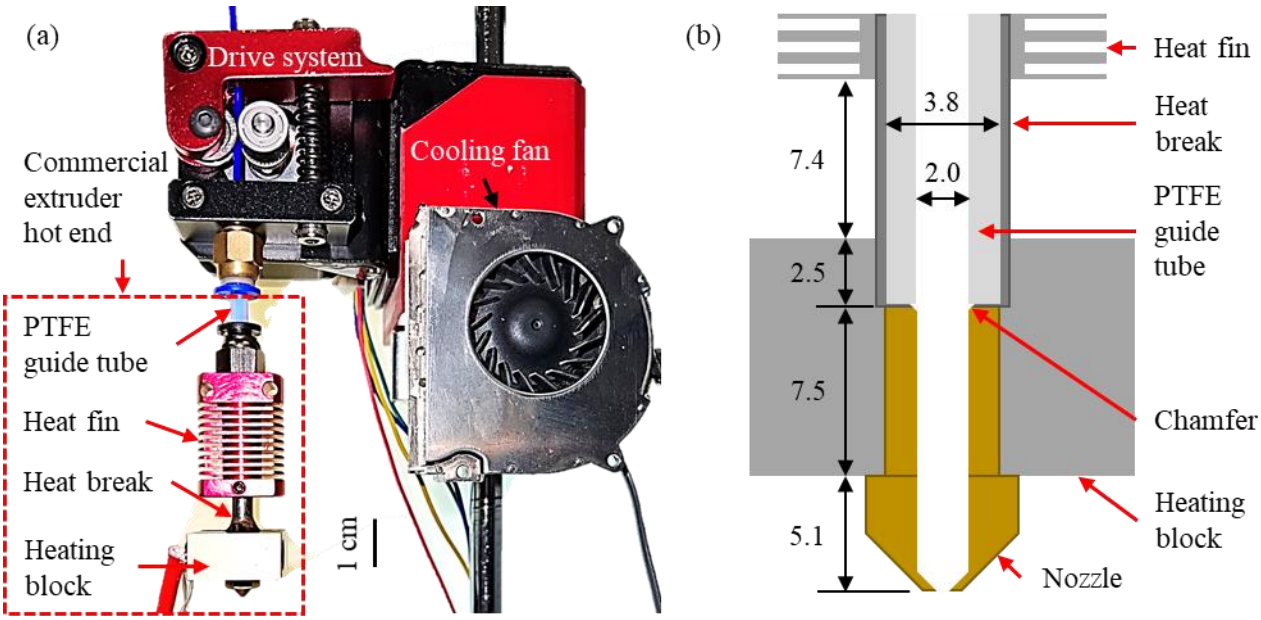


*Figure 8. Experimental setup for validation. (a) Experimental setup for validating the proposed gap-filling model, using a commercial extruder; and (b) illustration and dimensions of the commercial extruder. Units for dimensions are mm.*

The commercial extruder had five major components: a guide tube, a heat fin, a heat break, a tubular heating block, and a nozzle. The guide tube, which had an inner diameter of 2.0 mm, was used to facilitate the movement of a solid filament into the nozzle. This tube was located inside the tubular heat break. Part of the heat break was screwed into the heating block to connect the PTFE tube with the nozzle. The nozzle was heated to the extrusion temperature by the surrounding heating block. The nozzle was made of brass, while the heating block was made with aluminum. Both materials have high thermal diffusivity, which was designed to increase the heat conductivity to the nozzle. The temperature above the heating block was reduced through three approaches. First, the tubular heat break that sat the guide tube was made with stainless steel. As the thermal diffusivity of stainless steel at 4.26 – 7.25 [37] is ~ 6.4 – 15.1 % of that of aluminum at 48.0 – 66.6 [37], the tubular heat break is not effective in transferring heat upwards from the

heating block. Second, the heat fin was also made of aluminum. As such, the heat fin can quickly dissipate the heat that it received from the heating block through the heat break, into the air. Third, the guide tube was made of Polytetrafluoroethylene (PTFE). PTFE has a thermal diffusivity of 0.1 – 0.3 $mm^2/s$ [38], which is lower than that of borosilicate glass (0.8 – 0.9 $mm^2/s$ [39]) and much lower than those of brass (34.1 $mm^2/s$ [37]) and aluminum. Accordingly, this tube was designed not as effective in transferring the heat upward towards the heating block.

Both ABS and PLA filament extrusion tests were conducted using this validation setup (Figure 8(a)). The results are presented in Figure 8. These tests had the same process parameters as their counterparts shown in Figure 12 and Figure 13. The first type of tests was used to validate the first two step of the gap-filling process proposed in Figure 11. In a test, after the filament had been partially inserted inside the straight portion of the nozzle but had not reached the conical portion of the nozzle, the extrusion stopped. The heater for the heating block was then turned off, followed by using an additional air compressor (Central Pneumatic 92403, Cheyenne, WY, USA) to blow room-temperature air towards both the heat break and heating block to accelerate the cooling process. The air flow speed from the air compressor was measured to at 2.6 – 2.8 m/s. It could reduce the temperature from ~ 200 °C to 30 °C in about 1 min. When the extruder was cooled to room temperature, the filament was retrieved by dissembling the extruder. As in the cases of Figure 12 and Figure 13, the filling level on the retrieved filament was marked as *B* (Figure 9). The second type of tests was applied to examine the third step. In a test, before a sample was retrieved in a manner similar to that in the first type of test, it had gone through the entire nozzle and reached its steady state of extrusion. Its filling level was marked as *C*, as in the cases of Figure 12 and Figure 13.

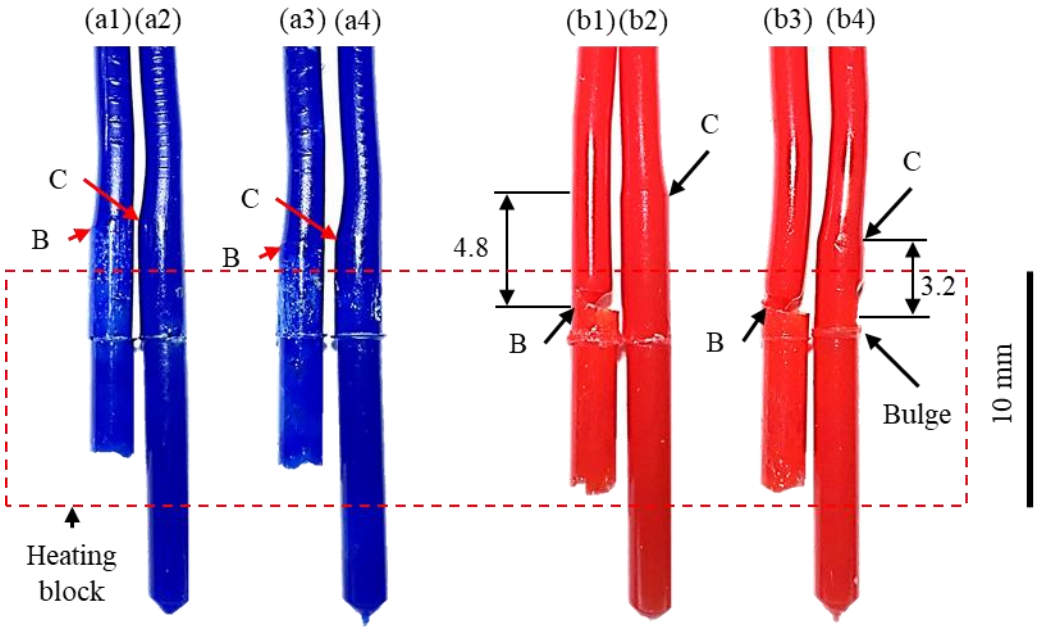


*Figure 9. Experimental validation of gap-filling results. Extrusion of ABS at $T_e$ = 230 °C for (a1, a2) U = 1.0 mm/s, and (a3, a4) U = 2.5 mm/s, respectively; and extrusion of PLA at $T_e$ = 210 °C for (b1, b2) U = 0.5 mm/s, and (b3, b4) U = 1.5 mm/s, respectively. Units for dimensions are mm. (a1), (a3), (b1) and (b3) are the samples obtained out of the first type of tests, and (a2), (a4), (b2) and (b4) are the ones the samples produced by the second type of tests. Bulge in each sample was induced by the chamfer at the interface of PTFE tube and nozzle (see Figure 8(b)), and it was used to align the samples at the same level.*

Two results were observed from the testing samples (Figure 9). First, all of the four samples obtained in the first type of test on ABS and PLA widened their bottom portions, which were the portions located below *B* (Figure 9 (a1), (a3), (b1) and (b3)). This result indicated that the gap-filling started in the straight part of the extruder's tube, and that it continued as the polymer moved down inside this portion. Second, in the second type of tests, all of the four samples, as shown in Figure 9 (a2), (a4), (b2) and (b4), had higher filling levels than their counterparts in the first type of tests. This can be seen from the height difference between *B* and *C* (Figure 9). The

difference was small (less than 1 mm) in the case of ABS (Figure 9 (a)), while it was large (more than 3 mm) in the case of PLA (Figure 9 (b)). This result shown that, as the polymer got into the conical portion of the nozzle, the nozzle's inclined wall caused the increase in the gap-filling level. These two results validated our proposed filling model.

## 3.4. Numerical Simulation of Steady State Filament Extrusion

### *3.4.1. Simulation Model & Assumptions*

The in-situ observation of the polymer flow is in line with non-Newtonian lamina flow. The fluid model was selected based on the in-situ obversions of steady extrusion process discussed in section 4.5.1. Figure 10 illustrates the geometry and boundary conditions implemented in ANSYS Fluent [40] for the present study. The simulation geometry was modeled closely based on the experimental setup, which included the lower heated section of the glass tube, as well as the filament melt inside the tube.

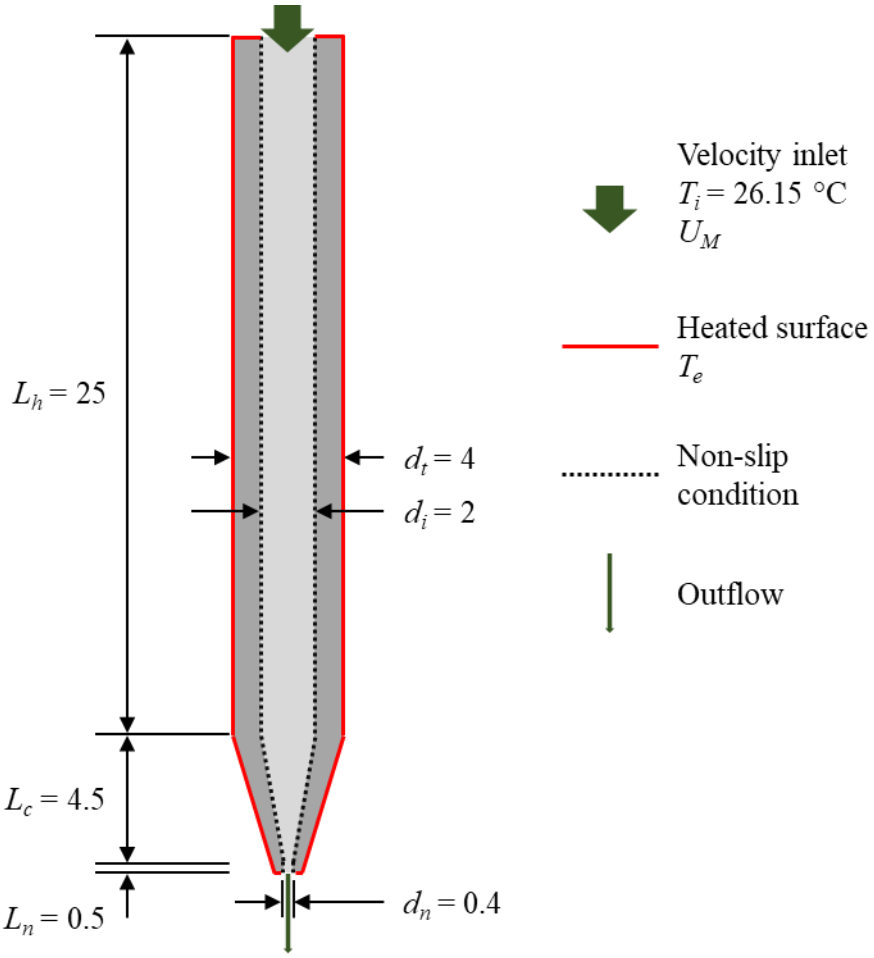


*Figure 10 Illustration of geometry of the numerical model and boundary conditions. Dimension unit in millimeter.*

The outer surface temperature of the tube, $T_e$ is set to be the same as the measured chamber temperature, $T_e$. The heated tube length, which is $L_h + L_c + L_n$, was defined in the presented model. The polymer flow was assumed to fill the entire heated tube, as our study [41] shows that the polymer flow filled at least 90% of the heated tube in steady extrusion conditions (section 4.2), and other existing thermal or pressure models [13, 14, 15, 16, 17].

The filament enters the tube in ambient temperature. The diameter of the entering filament was assumed to be the same as the inner diameter of the tube. Hence, in the simulation, the

filament entered the tube at modified feed rate $U_M$, instead of the filament feed rate $U$. This relation can be described with conservation of mass (Equation 1),

$$d^2U = d_i^2 U_M \tag{1}$$

where $d$ and $d_i$ are the diameter of the filament and inner tube, respectively.

Non-slip condition was applied between filament flow and glass tube inner wall. The filament travels the full length of the heated tube and extrudes via the conical nozzle which was set as outflow.

*3.4.2. Governing Equations*

In the simulation, a set of conservation of mass and momentum equations with an additional energy equation were solved using Finite Volume Method (FVM). The coupled system of equations was solved with the pressure-based coupled algorithm.

1) The mass conservation:

$$\frac{\partial \rho}{\partial t} + \nabla \cdot (\rho \boldsymbol{v}) = S_m \tag{2}$$

where $\rho$ is density of the fluid and $\boldsymbol{v}$ is the velocity vector. $S_m$ is the mass added to the continuous phase, for the present work, this term is 0.

2) The conservation of momentum:

$$\rho \frac{\partial \boldsymbol{v}}{\partial t} + \rho(\boldsymbol{v} \cdot \nabla \boldsymbol{v}) = -\nabla p + \nabla \cdot (\bar{\bar{\tau}}) + \rho \boldsymbol{g} + \boldsymbol{F} \tag{3}$$

where $\rho \boldsymbol{g}$, the gravitational body force was neglected and external body force $\boldsymbol{F}$ is 0.

$\bar{\bar{\tau}}$ is stress tensor given by Equation 4,

$$\bar{\bar{\tau}} = \mu\left[(\nabla \boldsymbol{v} + \nabla \boldsymbol{v}^T) - \frac{2}{3}\nabla \cdot \boldsymbol{v} I\right] \quad (4)$$

where $\mu$ is the molecular viscosity and $I$ is the unit tensor.

3) The energy equation:

$$\frac{\partial}{\partial t}(\rho \boldsymbol{E}) + \nabla \cdot [\boldsymbol{v}(\rho \boldsymbol{E} + p)] = \nabla \cdot \left( k_{eff}\nabla T - \sum_j h_j \boldsymbol{J_j} + \bar{\bar{\tau}}_{eff} \cdot \boldsymbol{v} \right) + \boldsymbol{S_h} \quad (5)$$

where $k_{eff}$ is the effective thermal conductivity. $\boldsymbol{S_h}$ is for volumetric heat sources, which is not apply in the presented work. $\boldsymbol{J_j}$ si the diffusion flus of species $j$.

The $\boldsymbol{E}$ in Equation 5 is given as,

$$\boldsymbol{E} = h - \frac{p}{\rho} + \frac{v^2}{2} \quad (6)$$

for incompressible flow, $h = \sum_j Y_j h_j + \frac{\boldsymbol{p}}{\rho}$, the $Y_j$ is the mass fraction of species $j$, and $h_j$ is given as,

$$h_j = \int_{T_{ref}}^{T} c_{p,j} dT \quad (7)$$

where $T_{ref}$ is 298.15 K

*3.4.3. Material Properties of the Tube*

The tube material properties modeled in the simulation were treated as constant, since the temperature dependency of these properties is negligible. Material properties of both borosilicate glass and aluminum are listed in

Table *3*. The thermal diffusivities of the tube materials were calculated (Equation 8) with these provided constants.

$$\alpha = \frac{k}{\rho C_p} \tag{8}$$

*Table 3. Material properties of borosilicate glass and aluminum*

| Property | Units | Borosilicate glass | Aluminum | Reference |
|---|---|---|---|---|
| Specific heat capacity ($C_P$) | *J/kg-K* | 779.74 | 895.61 | [42] |
| Thermal conductivity ($k$) | *W/m-K* | 1.1489 | 236.49 | [42] |
| Density ($\rho$) | $g/cm^3$ | 2.1249 | 2.6998 | [42] |
| Calculated thermal diffusivity ($\alpha$) | $m^2/s$ | $6.934\times10^{-7}$ | $9.781\times10^{-5}$ | Calculated |

*3.4.4. Material properties of the ABS*

We adopted the rheological property of ABS published in Seppala et al. [9] in our numerical simulation. The horizontal shift factor was fitted with Williams-Landel-Ferry (WLF) equation (Equation 9) valid in temperature range between 130 °C to 270 °C.

$$log(\alpha_T) = \frac{-C_1(T - T_r)}{C_2 + (T - T_r)} \tag{9}$$

where, $C_1$, and $C_2$ are material constant WFL equation, and $T_r$ is reference temperature. Then, the temperature dependent viscosity, $\eta$, can be descript as (Equation 10)

$$\eta(T) = \eta_r \alpha_T(T) \tag{10}$$

where, $\eta_r$ is the consistency index at reference temperature, and $\alpha_T(T)$ is the horizontal shift factor at temperature, *T*.

The rheological properties and other material constants of ABS used in our numerical simulation are organized in Table 4. Thermal diffusivity of ABS was calculated (Equation 8) with these provided constants.

*Table 4. Material properties of ABS used in numerical simulation*

| Property | Units | Value Range | Reference |
|---|---|---|---|
| Reference temperature ($T_r$) | $°C$ | 230 | [9] |
| Glass transitional temperature ($T_g$) | $°C$ | 100, 104.5 | [43, 9] |
| Specific heat capacity ($C_P$) | $J/kg\text{-}K$ | 1863 | [43] |
| Thermal conductivity ($k$) | $W/m\text{-}K$ | 0.205 | [43] |
| Density ($\rho$) | $g/cm^3$ | 1.216 | [43] |
| Consistency index ($\eta_r$) | $Pa.s$ | 10400 | [9] |
| Power-law index ($n$) | - | 0.32 | [9] |
| WLF constant 1 ($C_1$) | - | 4.65 | [9] |
| WLF constant 2 ($C_2$) | $°C$ | 200.9 | [9] |
| Thermal Diffusivity ($\alpha$) | $m^2/s$ | $9.049\times10^{-8}$ | Calculated |

# CHAPTER 4

# RESULT & DISCUSSION

## 4.1. Transient Extrusion Process in an Initially Empty Tube

### *4.1.1. Observed Gap-Filling Procedure*

When a solid filament is inserted into an empty tube, the aforementioned gap mainly existed in the cylindrical session of the tube. In the conical nozzle, the inner diameter of the tube quickly reduced to be less than the diameter of the solid filament.

In our extrusion tests on both ABS and PLA, no distinctive difference is observed between the gap-filling processes, although they are different materials. For both ABS and PLA filaments, a gap-filling is found to be affected by three factors: i) contact of the filament with the tube wall, ii) the temperature of the polymer in the neighborhood of the contact site, and iii) the flow of polymer melts around the contact site. The combinative effect of these three factors makes the gap filled through three steps, as illustrated in Figure 11 and shown in Figure 12 – Figure 14, and supplementary videos 1 – 6. Extrusion temperatures of 230 °C and 210 °C are commonly used for ABS and PLA, respectively. All (a) of Figure 12 – Figure 14 are representative gap-filling processes in the case of ABS. They are observed when the extrusion temperatures are fixed to be 230 °C, while the feed rates are 1.0, 2.5, and 5.0 mm/s, respectively. The images in (a) of Figure 12 – Figure 14 are, respectively, extracted from supplementary videos 1, 3, and 5. All (b) of Figure 12 – Figure 14 are representative gap-filling processes in the case of PLA. They are observed when the extrusion temperatures are fixed to be 210 °C and the feed rates are 0.5, 1.5, and 3.0

mm/s, respectively. The images in these figures are, respectively, extracted from supplementary videos 2, 4, and 6.

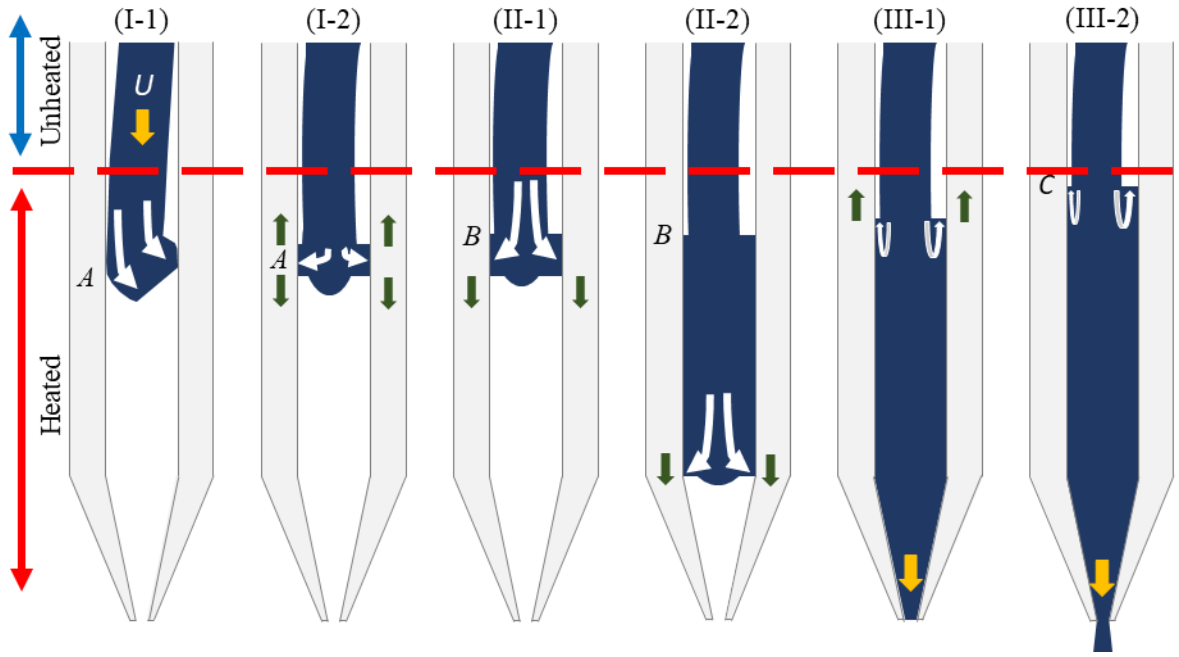


*Figure 11. Illustration of three-step gap-filling process during the transient stage of extrusion. (I-1) filling at the lowest contact site, and (I-2) spreading around the contact sites; (II-1) and (II-2) spreading downwards until the filament front reaches the end of straight section of tube; and (III-1) and (III-2) further rise of the filling level as the polymer gets to the conical nozzle. "A", "B", and "C", respectively, mark the initial, intermediate, and final gap-filling levels. Thick red arrows denote the gap-filling directions, and white arrows represent flow directions. The same labelling applies to the following figures.*

The observed gap-filling process that is illustrated in Figure 11 is different from what are proposed in [10, 11, 12]. In these two references, the filament is assumed to be straight, and it did not contact the tube wall until the filament front reached the conical nozzle. The polymer melt,

that is generated due to the direct contact with the inclined wall of the conical nozzle, then flowed upwards to fill the gap in the straight portion of the heated tube. However, as detailed below, according to our observation, the gap-filling starts at a different location, and the filling process is more complicated than what are proposed in other studies [10, 11, 12].

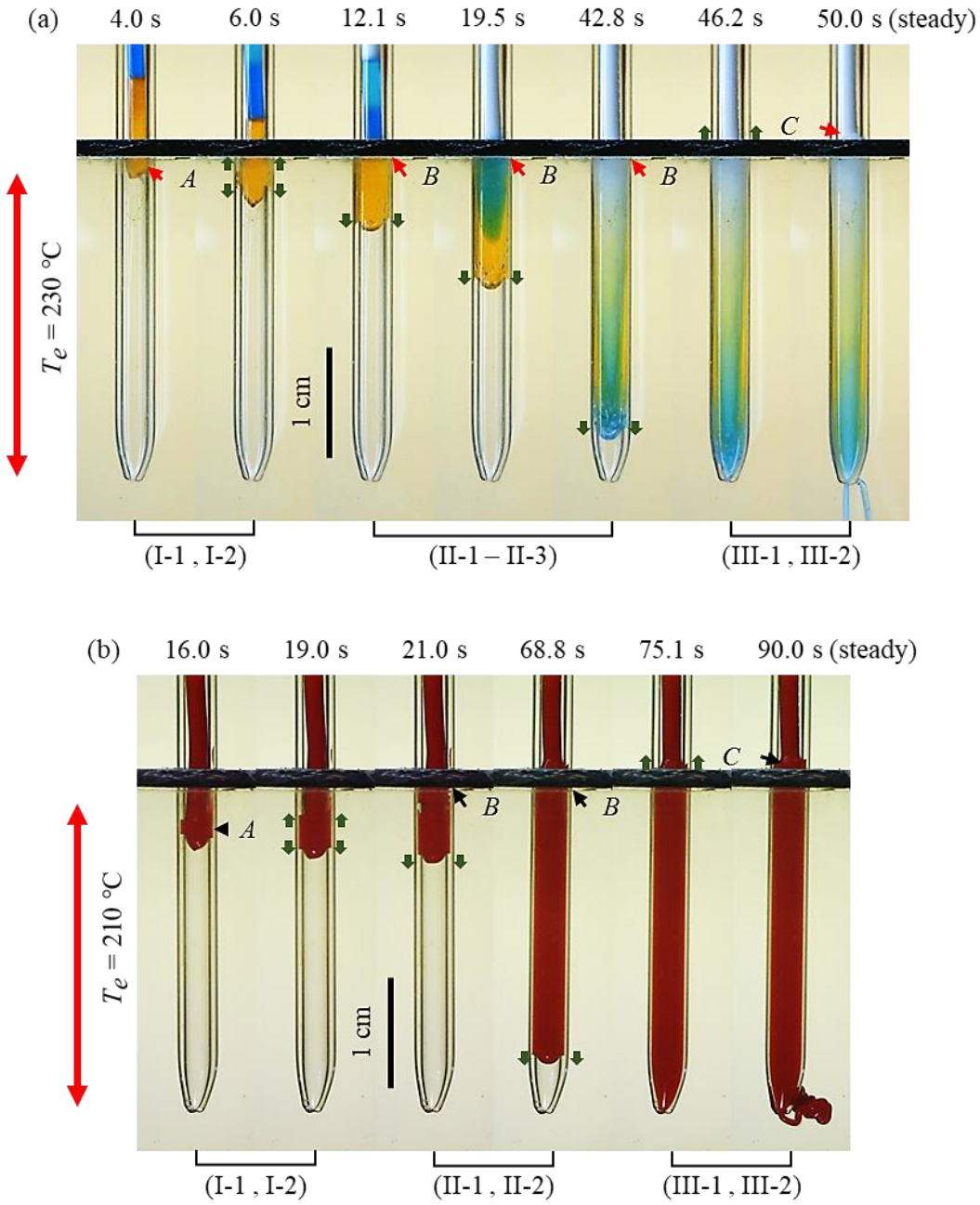


*Figure 12. Over-filled filament extrusion case. (a) $T_e$ = 230 °C and U = 1.0 mm/s for ABS, and (b) $T_e$ = 210 °C and U = 0.5 mm/s for PLA.*

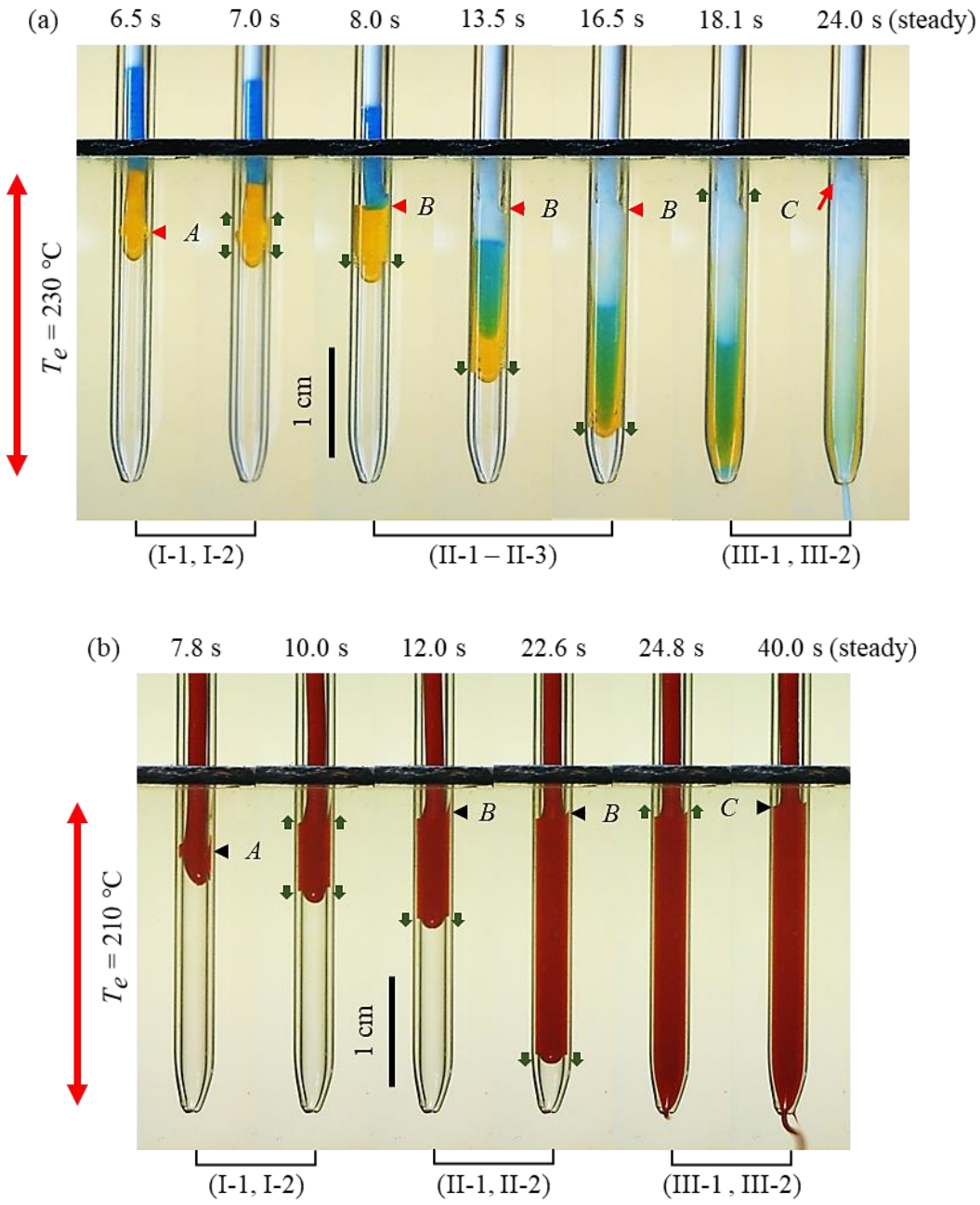


*Figure 13. Partial-filled filament extrusion case. (a) $T_e$ = 230 °C and U = 2.5 mm/s for ABS, and (b) $T_e$ = 210 °C and U = 1.5 mm/s for PLA.*

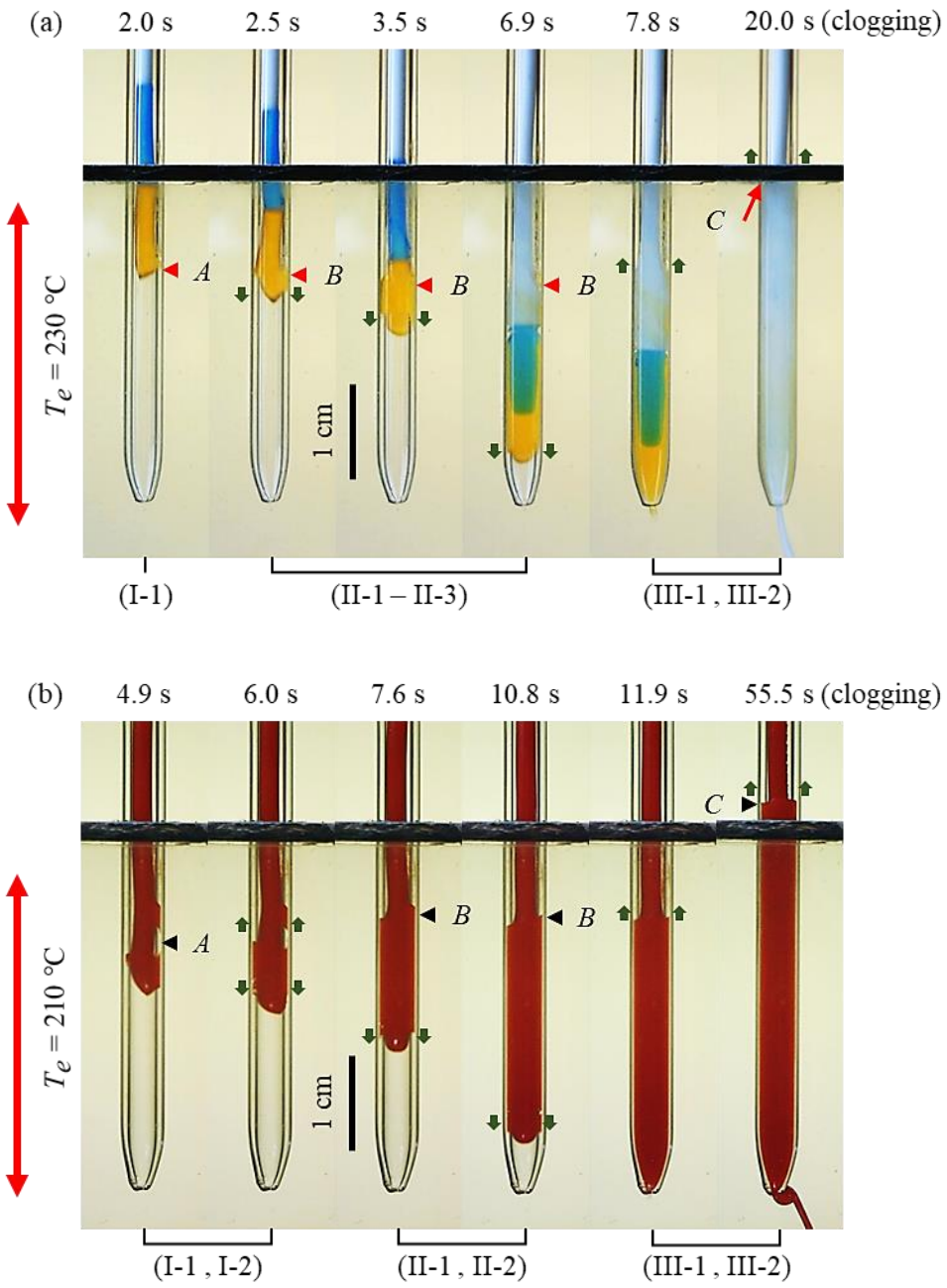


*Figure 14. Clogging filament extrusion case. (a) $T_e$ = 230 °C and U = 5.0 mm/s for ABS, and (b) $T_e$ = 210 °C and U = 3.0 mm/s for PLA.*

*4.1.2. The Three Step of Gap-Filling Model*

In the first step, the gap-filling starts at the edge of the filament front (Figure 11 (I-1)). The filament that comes off from a reel has a curved shape. Owing to this shape, when it is fed into the tube, the edge of the filament front has direct contact with the tube wall, as shown in Figure 6(a) and (I-1) of Figure 12 – Figure 14. The part of the filament, which is not in contact with tube wall, receives heat from the tube wall through air in the gap. In contrast, at the contact site, the polymer receives heat directly from the tube wall through conduction, which is more effective in transferring heat. Furthermore, the filament front enters the heated tube first. It is heated longer than the other portion of the filament. As such, the temperature of the polymer at the edge of the filament front, which is in the contact with the tube wall, quickly rises to $T_c$. The corresponding polymer melt sticks to the tube wall. Once the gap with a length of approximately 1 mm is filled, the filling phenomenon can be visually identified according to its distorted image. The location is marked as *A* in (I-1) of Figure 11 – Figure 14, where the gap-filling begins to happen.

The increase in the contact area between the filament and tube wall around *A* accelerates the melting process. When the feed rate is not high, the polymer melt produced around *A* may spread both upwards and downwards along the tube wall to fill the gap located below and above *A* (see, for example, (I-2) of Figure 12 and Figure 13). This spreading is considered to be propelled by the filament's solid core, which functions as a plunger to drive the surrounding polymer melt to move aside. When the feed rate is high, the polymer melt may not spread upwards around *A*. For example, at $T_e$ = 230 °C, when the feed rate is 5.0 mm/s, the molten polymer spread downwards around *A* (Figure 14 (a)). These observations indicate that there is a balance between the local backflow speed of the polymer melt and the feed rate of the filament. As the feed rate is higher

than the backflow speed, the polymer melt only spreads downwards along the tube wall. Otherwise, it spreads both upwards and downwards.

If the polymer flows upwards along the tube wall, then the gap-filling level is raised. This new gap-filling level is denoted by *B*, as shown in (II-1) of Figure 11 – Figure 13. For simplicity in description, in case there is no rise in the gap-filling level, the corresponding gap-filling level is still marked by *B* ((II-1) of Figure 14 (a)). Subsequently, the second step of gap-filling starts. When the filament front continues to move down in the straight session of tube, the gap-filling level remains approximately at *B*. Meanwhile, as the filament front moves down, the gap around the filament front is filled simultaneously by the polymer melt.

As shown in (a) of Figure 12 – Figure 14, in the case of ABS, the orange section of the filament enters a heated tube first. It receives heat from tube wall longer than the latter section (blue). Thus, the orange polymer melts before the blue one. Storage modulus of ABS decrease with the increase in temperature [44] (also true for PLA [45]). Accordingly, the blue section of the filament functions as a plunger to push the orange polymer to fill the gap located below *A*. This point can be seen clearly from (II-1 – II-3) of Figure 13 (a) and Figure 14 (a), when the feed rates are relatively high. They are 2.5 and 5.0 mm/s, respectively. The blue section of the filament is not much deformed. It still had an approximately rectangular shape. This shape indicates that the blue section is still in solid phase, enabling it to function as a plunger to push the orange polymer melt aside.

The third step begins when the filament front reaches the conical portion of the tube. In this step, the filament front moves through the conical nozzle and then exits from the tube's opening. During this step, the filament receives an additional resistance from the inclined tube wall. This resistance decreases the moving speed of the filament in the straight portion of the tube.

To maintain the feed rate, the feed force is increased. This increases the force that is applied by the solid core of the filament to push its surrounding polymer melt at *B*. Accordingly, once the filament gets to the conical nozzle, the gap-filling level starts to rise again ((III-1) of Figure 11 – Figure 14). As illustrated in Figure 11(III-1), the corresponding filling mechanism is similar to the one that causes the rise of the gap-filling level from *A* to *B* in the first step (Figure 11(I-2)). As observed from (III-2) of Figure 12 – Figure 14 (a), the newly filled gap is filled by the white polymer melt, instead of blue or orange one. Therefore, different from what has been previously assumed in [10, 11], the polymer melt that fills the gap in this step does not come from the bottom of the tube. Instead, it is from the portion of the filament that passes by *B*. This filling phenomenon matches the simulation result of [12]. The final gap-filling level is denoted by *C*, as shown in (III-2) of Figure 11 – Figure 14. When the extrusion reaches its steady state, *C* remains at about the same level as the extrusion continues ((III-2) of Figure 12 and Figure 13 and video 1 – 4). However, in the case of clogging, due to the continued increase in the feed force, the location of *C* keeps moving up ((III-2) of Figure 14, and video 5 and 6), until the driving gears slip.

The diameter of an ABS or PLA filament may not be exactly 1.75 mm. As indicated by their manufacturer, this size may vary by ± 0.05 mm. However, this size variation has a much less effect on the gap size, in comparison with the curved profile of the filament. A free-standing filament has a lateral deflection with the order of 1 cm at its tip, which is much larger than the diameter variation. Also, it is observed in our tests: i) the gap-filling starts at the location where the filament tip has contact with the tube wall, and ii) the filling continues, as the polymer melts spread around the contact sites. The diameter variation is not the main factor to decide whether a filament contacts the tube wall. Therefore, it is negligible in considering gap filling.

## 4.2. The Three-Filling Process Regions

For different combinations of extrusion temperature and feed rate, according to the final level that the gap is filled and the occurrence of clogging, three filling regions are found (Figure 15): over-filled, partial-filled, and clogging. Figure 12 – Figure 14 give the examples of these three regions, respectively.

Steady-state extrusion is sustainable in both over- and partial-filled regions. The final gap-filling levels in the over- and partial-filled regions are located above and inside the observation chamber, respectively. With extrusion temperature fixed, the over-filled case mainly occurs due to its feed rate, which is lower than those in the other two cases. This feed rate makes the polymer located at the contact site receive enough heat to melt soon after it gets into the heated tube. Consequently, the gap-filling starts at a location near the entrance of the heated tube (Figure 12). The gap-filling level further rises to above the chamber by the driving force of the filament's solid core. The temperatures above the chamber are much lower than that inside the heated section of the tube. Consequently, the polymer melt located above the chamber in an over-filled case quickly cools down.

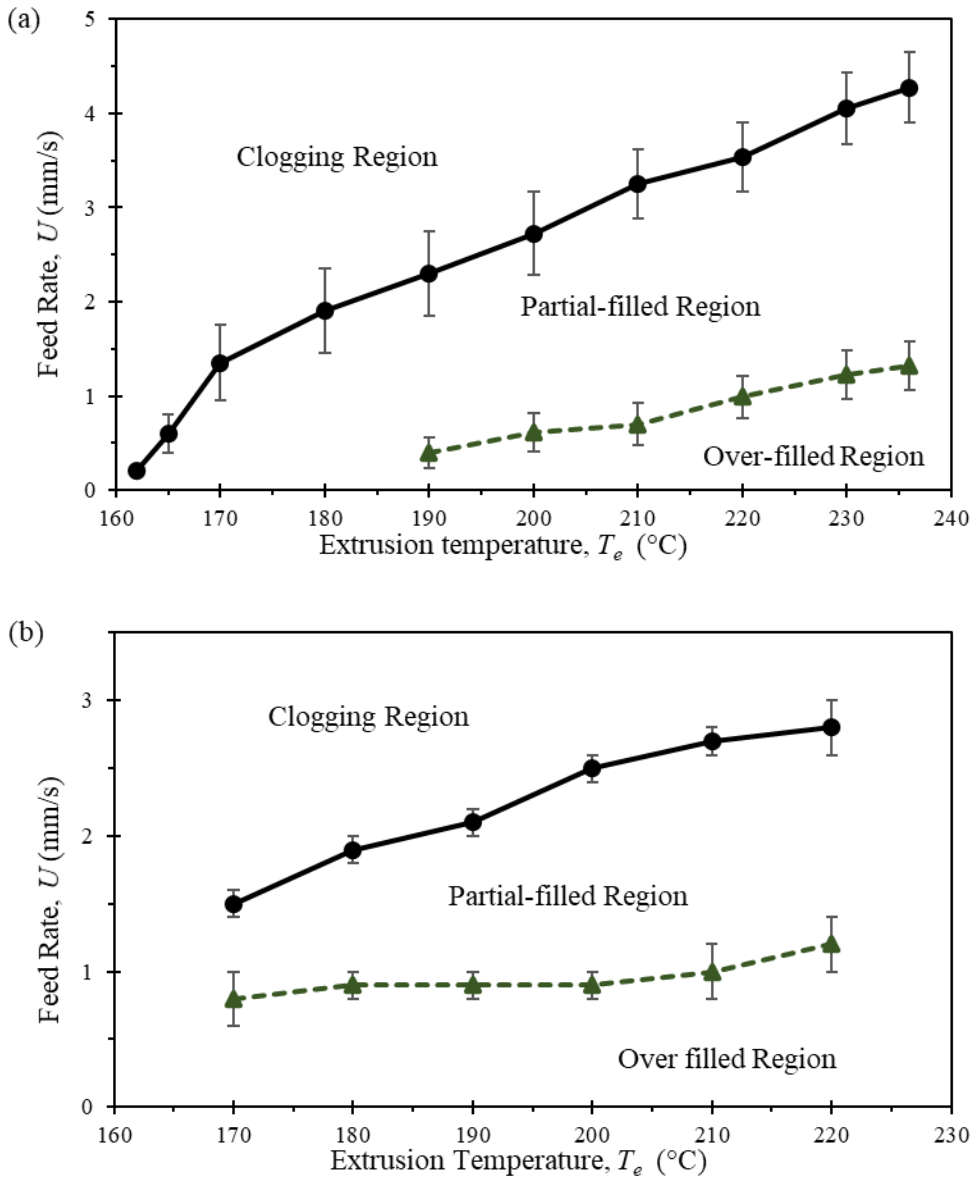


*Figure 15. Experimentally determined three gap-filling regions. (a) ABS and (b) PLA.*

The viscosities of both ABS [13] and PLA [26] increase with the decrease in temperature. As such, the portion of the polymer above the chamber provides a shear stress much larger than that the filament encounters inside the heated tube. After the extrusion stops, this portion of the polymer is solidified. It may form a seal around the filament to stop the insertion of the filament when the extrusion re-starts. In a partial-filled case (Figure 13), since the feed rate is relatively

high, the gap-filling begins at a point away from the entrance of the heated tube, making the final filling level below the chamber. Accordingly, there is no extra shear stress produced at the entrance of the heated tube. In a clogging case (Figure 14), the extrusion fails. According to the above discussions, a partial-filled case may be preferred in MaxEx.

As observed from Figure 15, to avoid clogging and have a tube partially filled at a high feed rate, the corresponding extrusion temperature should also be high. Take ABS as an example, to make this case occur at $U$ = 3.5 mm/s, $T_e$ should be at least 235 °C. Moreover, according to Figure 15(a), when the extrusion temperature is in the range of 210 °C to 236 °C, which is part of extrusion temperatures used in a MatEx 3D printer to print ABS (210 °C to 260 °C) [9], the heated tube is partially filled by the polymer if the feed rate is between 1 and 2.5 mm/s. In addition, as observed from Figure 13, only less than 10% of the heated tube is not fully filled in a partial-filled case. This result indicates that, in the corresponding thermal or pressure model for stead-state extrusion, the tube could still be approximated as being fully filled, as what is done in [13, 14, 15, 16, 17].

Also demonstrated in Figure 15 is the difference between amorphous (ABS) and semicrystalline (PLA) polymers. In the case of PLA, even although the feed rate is small (e.g., 0.2 mm/s), steady extrusion could not be achieved until extrusion temperature increased to above its melting temperature (around 170 °C). Otherwise, clogging occurred. In the case of ABS, the critical temperature to have steady extrusion at a low feed rate (0.2 mm/s) is 162 °C. It is close to the corresponding temperatures reported in the literature, which are 160 °C [14] and 164 °C [16], respectively.

4.3. Transient Extrusion Process Sub-Case I – Change filament

*4.3.1. Removal of the Filament's Upper Portion*

In this sub-case, after the extrusion is paused, the driving system's direction is reversed to lift the upper portion of the filament from the glass tube at a constant rate of 2.5 mm/s (Figure 16 and their corresponding videos 7 and 8).

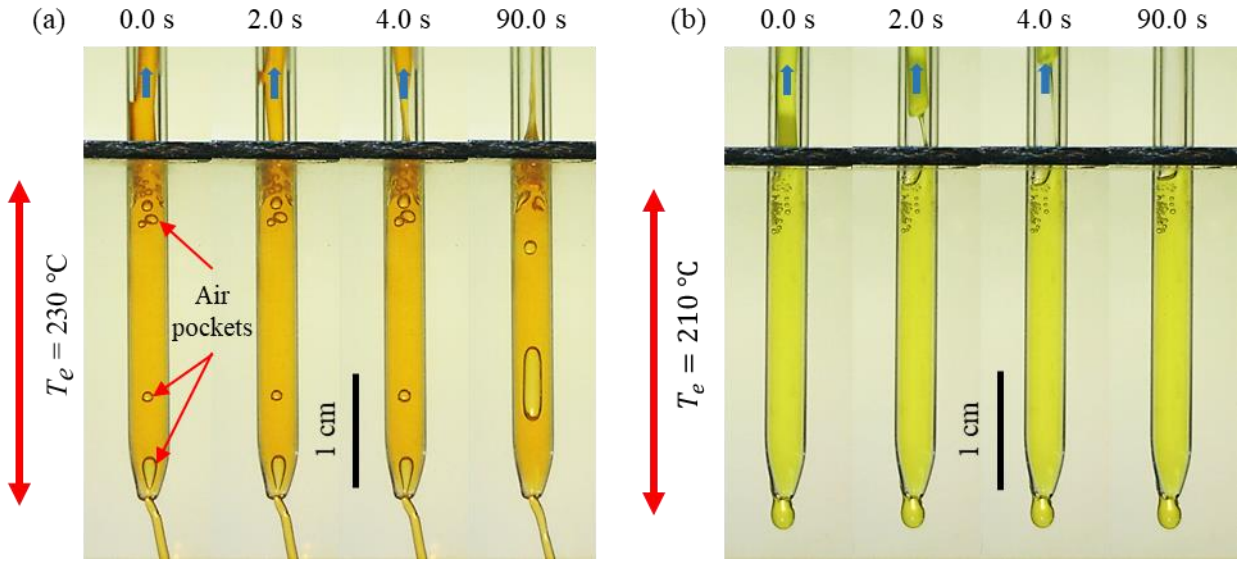


*Figure 16. Sub-case I – Removal of the filament's upper portion. (a) $T_e$ = 230 °C for ABS, and (b) $T_e$ = 210 °C for PLA. The removing speeds for both (a) and (b) were 2.5 mm/s.*

The bottom melted portion is left inside the heated section of tube. Air pockets are observed in the left polymer. They seemed to have random shapes and locations. These visible pockets are considered to originate from small air bubbles pre-existing inside a filament, or the air that had been trapped during prior gap-filling process. They are invisible during the prior gap-filling process, as they are compressed by feed force. Due to the removal of the upper section of

filament, these small bubbles are decompressed and gradually grew in size, as seen from Figure 16(a) and video 7. In the case of PLA, there is not much change in the bubble size during the removal of its upper portion (Figure 16(b) and video 8). A possible reason is that PLA relaxes its residual stress slower than ABS.

*4.3.2. Changing Filament*

A new filament is then inserted into the heated tube to resume the extrusion (Figure 17 and Figure 18, and their corresponding video 9 – 12). To distinguish with the polymer pre-existing in the heated tube, a filament with a different color is inserted. Two points are observed during the resumed extrusion. First, the gap-filling process is similar to the third step of the case considered in section 4.1 (Figure 11(III)). Second, the gap-filling level during steady extrusion returned to *C*, which is the gap-filling level before the extrusion had been paused ((III-2) of Figure 12 and Figure 13). These two points are seen clearly from Figure 17(a) and video 9. Before the extrusion is resumed, the gap-filling level, which is marked by *D* in the image of $t$ = 4.0 s in Figure 17(a), is lower than *C*. Part of the orange polymer originally inside the heated section of tube is taken away when the upper portion of the orange filament is removed from the tube. This caused *D* to be lower than *C* (Figure 17(a)). As the new filament insert is melted, part of the polymer melts around *D* flowed upwards, raising the filling level back to *C*. In the four examples considered in this study (Figure 17 and Figure 18), the final filling levels are about the same as their counterparts in steady-state extrusion ((III-2) of Figure 12 and Figure 13).

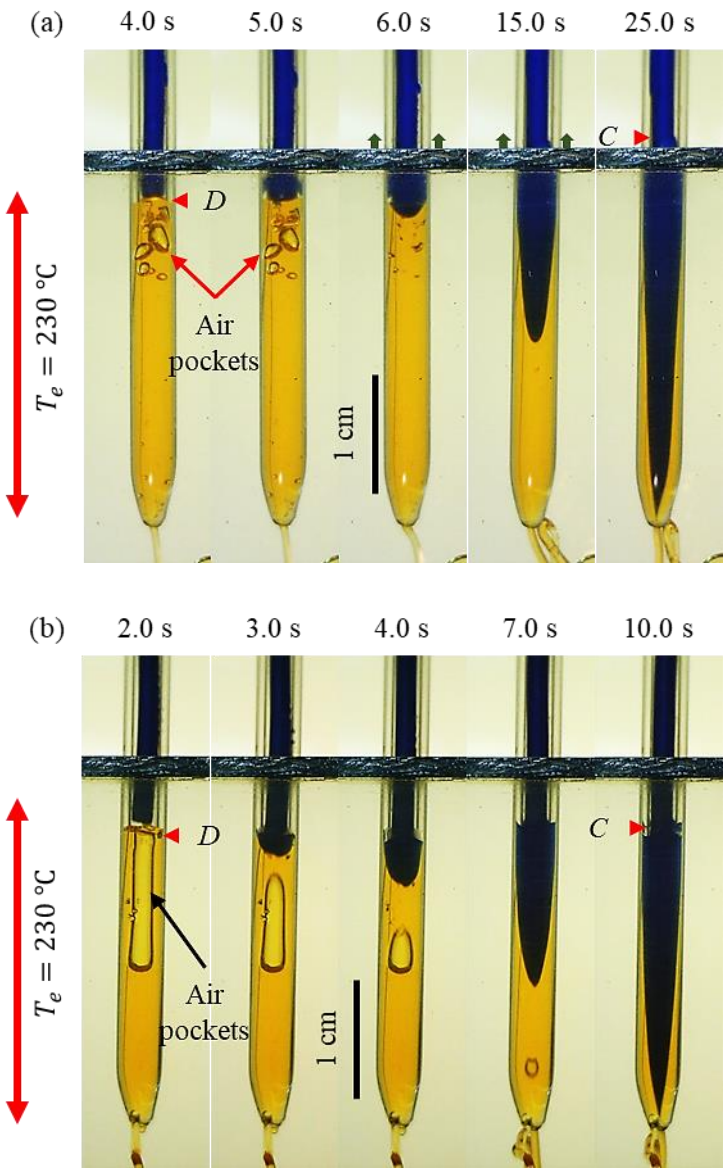


*Figure 17. Sub-case I – Change ABS filament at $T_e$ = 230 °C: (a) U = 1.0 mm/s, and (b)U = 2.5 mm/s.*

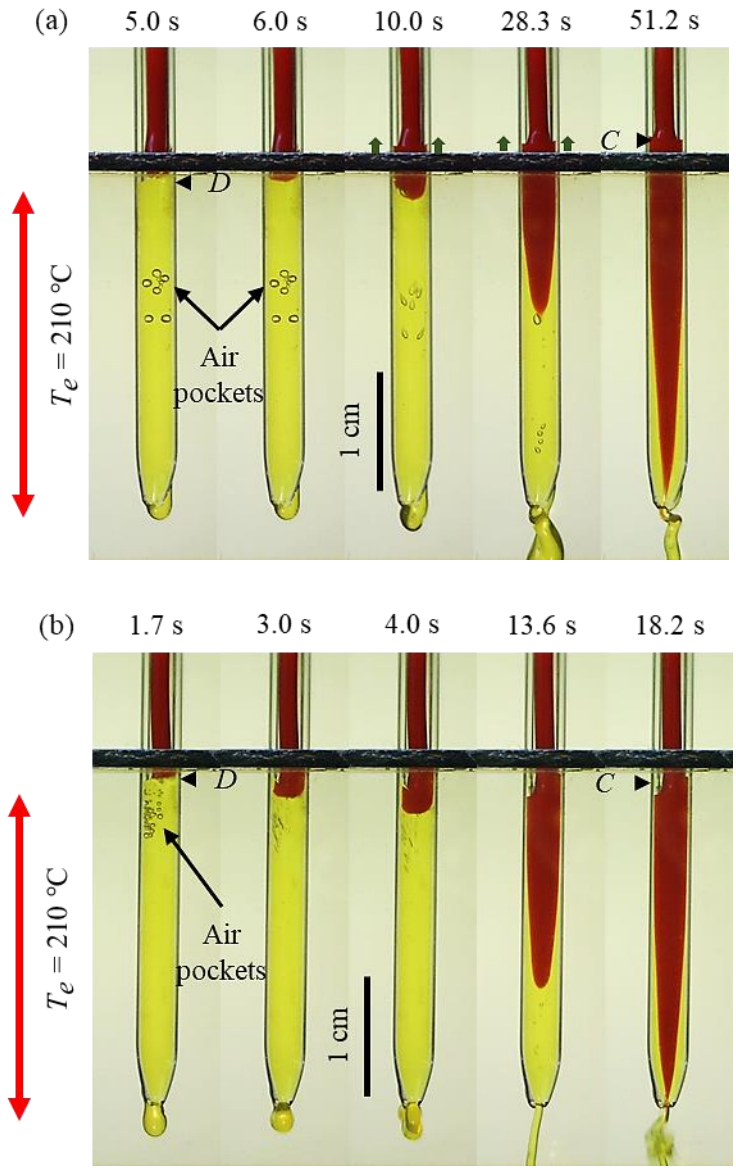


*Figure 18. Sub-case I – Change PLA filament at $T_e$ = 210 °C: (a) U = 0.5 mm/s, and (b) U = 1.5 mm/s.*

## 4.4. Transient Extrusion Process Sub-case II – Resume Extrusion

Resuming extrusion after a cool-down period is another common scenario in MatEx. To replicate this scenario, the steady-state extrusion is first stopped, and the setup is then cooled down. However, different from that in Sub-case I, in this subcase, the filament is not removed from the tube, and it is still kept inside. After the entire setup had been cooled down to room temperature for a while, the tube and filament are re-heated to extrusion temperature to resume extrusion. Extrusion temperature and feed rate are kept the same as those used in Sub-case I. Experimental results are given in Figure 19 and Figure 20.

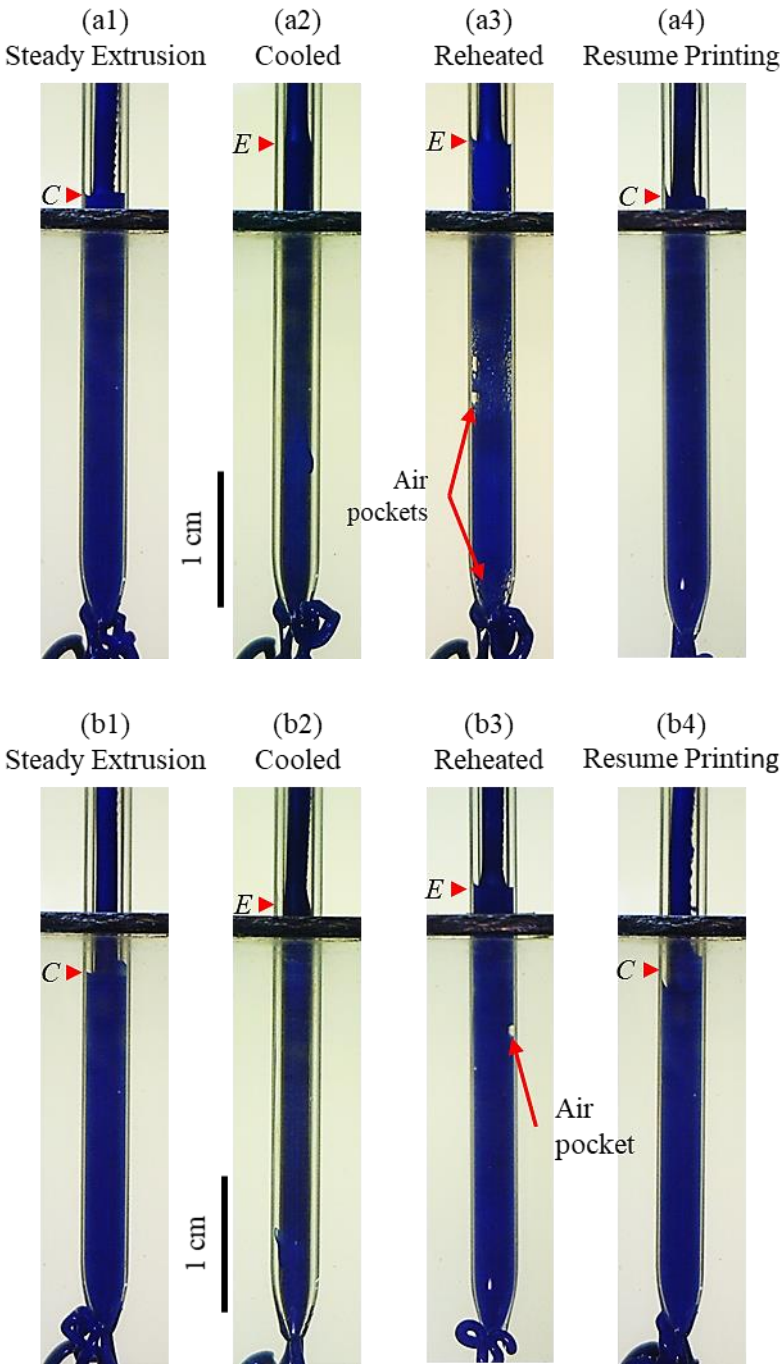


*Figure 19. Sub-case II – Resumed extrusion of ABS at $T_e$ = 230 °C: (a1 – a4) U = 1.0 mm/s, and (b1 – b4) U = 2.5 mm/s.*

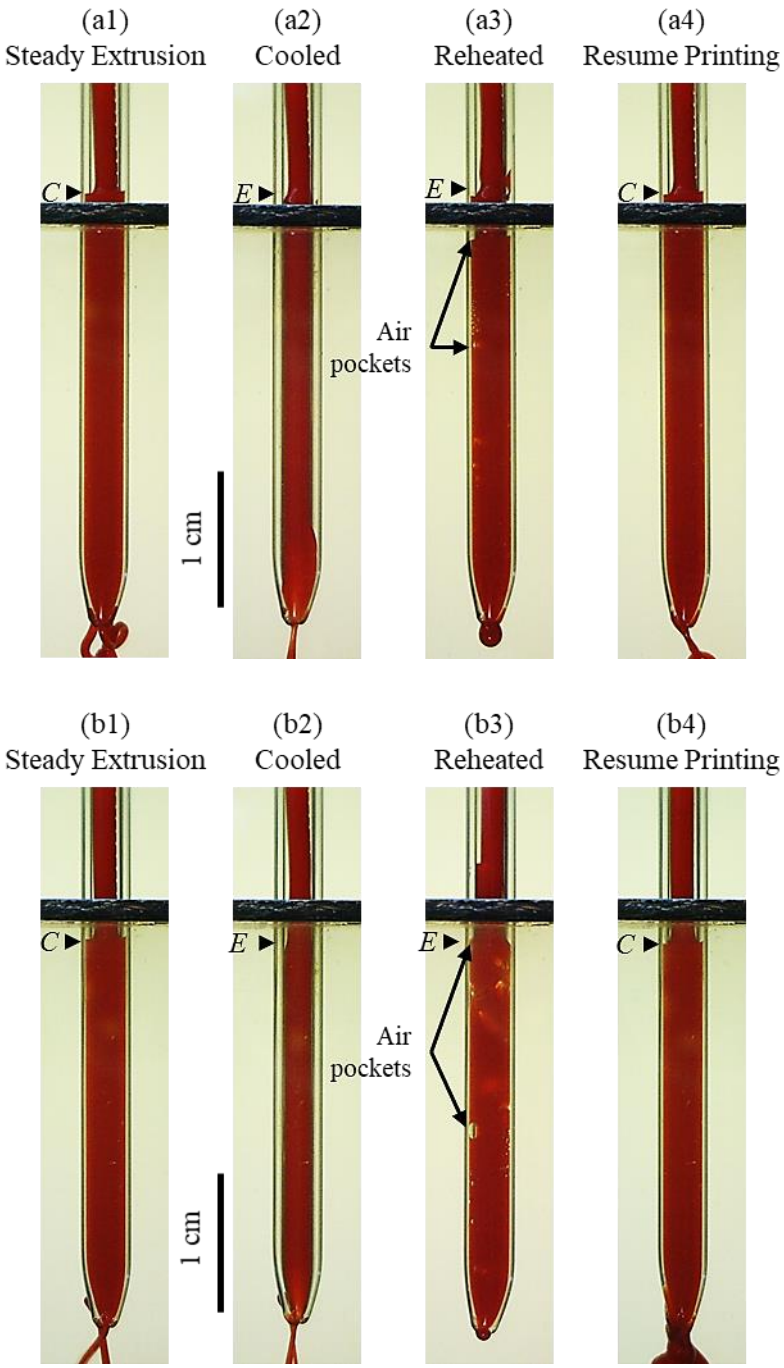


*Figure 20. Sub-case II – Resumed extrusion of PLA at $T_e$ = 210 °C: (a1 – a4) U = 0.5 mm/s, and (b1 – b4) U = 1.5 mm/s.*

As indicated below, four interesting phenomena are observed from Figure 19 and Figure 20.

First, when the temperature of the chamber gradually dropped down to room temperature, the filament shrank along its radial direction, as shown in (a2, b2) of Figure 19 and Figure 20.

Second, the polymer might either flow upwards or downwards during the cool-down period, depending on along which direction the polymer melt receives less resistance. As the surrounding environment decreases its temperature, the outer region of the filament cools down faster than its core (see, for example, [44] for a similar situation), which generates a thermal stress to squeeze the polymer melt in the core. Accordingly, the polymer melt should flow towards either the entrance or exit of the tube. The portion of the polymer located near the entrance of the heated tube cools down faster than that close to the nozzle, as this portion of the polymer is closer to the colder end of the tube. The corresponding temperature gradient may also generate a thermal stress. In the case of PLA, this thermal stress appeared to prevent the polymer melt from flowing upwards, while it drove the polymer melt out of the nozzle. Accordingly, the filling level of PLA inside the cooled tube, denoted as *E* in Figure 20(a2, b2), stayed at about the same as during steady-state extrusion. Meanwhile, PLA polymer is found to continue to move out of the nozzle during the cooling-down period. When the polymer had a high viscosity, the shear stress on the nozzle wall might prevent the polymer flowing out of the nozzle. This seems to be the case of ABS, in which the polymer mainly moved upwards. Consequently, during the cool-down period, the filling levels, which are denoted as *E* in Figure 19(a2, b2), rose to above the prior filling level *C*. When the temperature decreased from extrusion temperature (210 °C) to melting point (170 °C), the viscosity of PLA increased from about 100 Pa-s of 6 KPa-s [26]. In contrast, as the temperature lowered down from extrusion temperature (230 °C) to 164 °C (the critical temperature to avoid the

occurrence of clogging [16]), the viscosity of ABS increased from 10 KPa-s to 2 MPa-s [16]. Accordingly, as shear stress is proportional to viscosity, the viscous force that ABS experienced at the nozzle is at least 100 times that PLA encountered. Accordingly, ABS is difficult to get out of the nozzle during the cool-down period.

Third, when the entire setup is re-heated back to extrusion temperature, the polymer melt re-filled the gap between the edge of the filament and the tube wall, with air pre-existing in the gap trapped on the tube wall, as seen from (a3, b3) of Figure 19 and Figure 20. However, once the corresponding air pockets are pushed out from the tube during the resumed extrusion, no more air pockets are visible inside the tube.

Fourth and finally, as in Sub-case I, after the resumed extrusion reached steady state, the gap-filling level returned to its original level *C* (Figure 19 and Figure 20).

## 4.5. In-situ Observation of Steady Extrusion Process

### *4.5.1. In-situ Observation*

Figure 21 shows two selected filament steady extrusion cases in low (Figure 21(a) for $U$ = 0.5 mm/s) and high feed rate (Figure 21(b) for $U$ = 2.5 mm/s). For both cases, the extrusion temperature is set at $T_e$ = 230 °C. For both low and high feed rate cases, the solid filament filled the entire gap between filament and tube inner wall, as the cross-section of tube turned blue once the blue-colored section filament entered the heated portion (Figure 21 (a, b) at 5 s and 1 s, respectively).

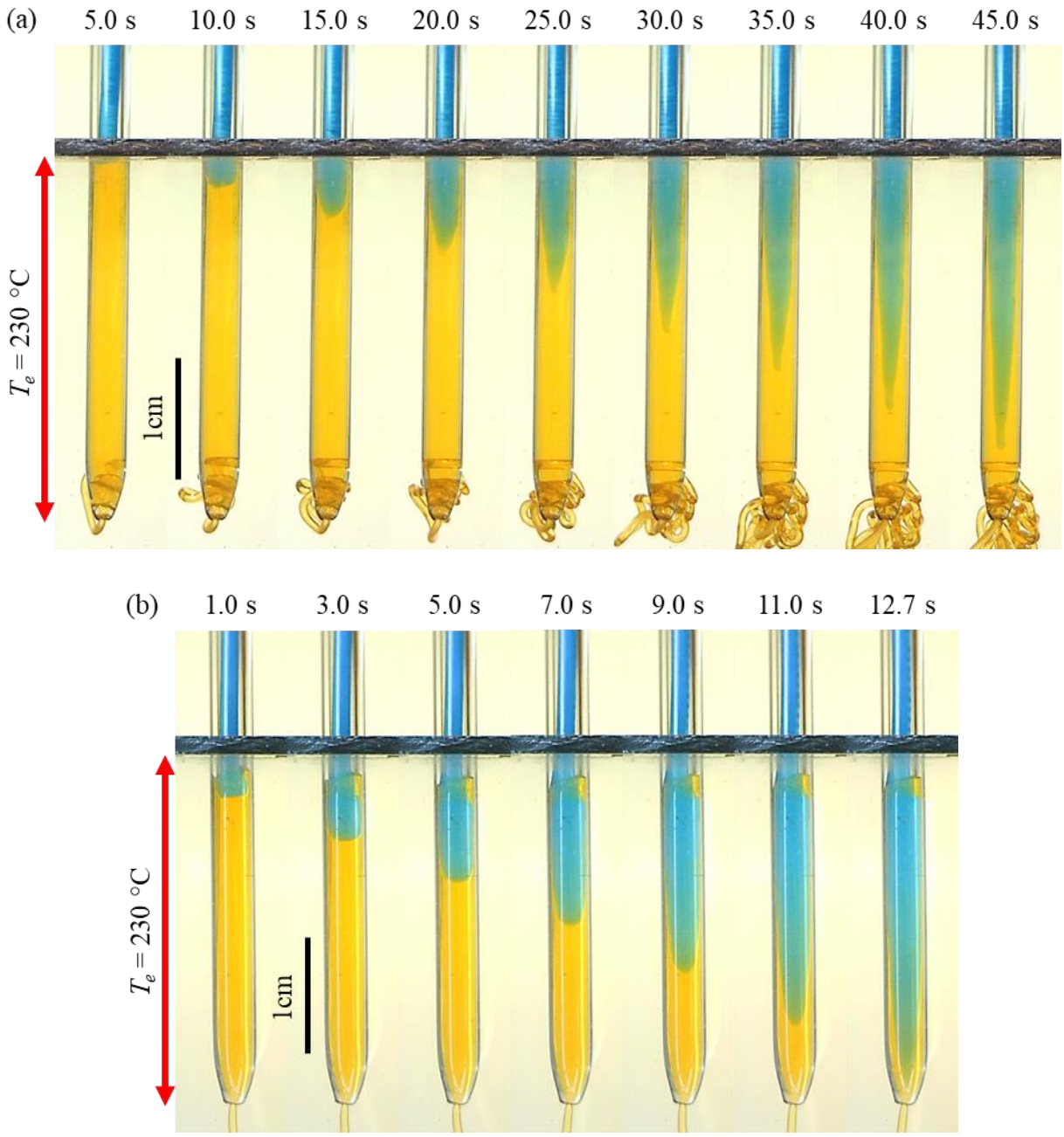


*Figure 21. ABS filament steady extrusion at $T_e$ = 230 °C, (a) U = 0.5 mm/s, and (b) U = 2.5 mm/s.*

The filling levels of polymer melt stays at the dynamic equilibrium level, and they are consistent with the gap-filling level at stage III-2 (III-2 of Figure 12 and Figure 13) discussed in section 4.1.1. In both cases, the boundary between the two different colored sections remained

clear throughout the extrusion process without signs of mixing. This flow characteristic is in line with the laminar fluid dynamics. We estimated the Reynolds number (Equation 11) of the polymer flow inside heated tube at below ~ $10^{-5}$ using the tube dimension and material properties listed in Figure 10 and Table 4 , respectively.

$$Re = \frac{V d_i \rho}{\mu} \tag{11}$$

where $V$ is flow velocity (~ $10^{-4}$ - $10^{-3}$), $d_i$ is tube inner diameter (~ $10^{-3}$), $\rho$ is density of the flow (~ $10^{3}$), and $\mu$ is the dynamic viscosity (~ $10^{3}$ – $10^{5}$). Our estimation is in the range of polished value in Serdeczny et al. [12], the low Reynolds number suggested laminar flow.

The difference between the low and high feed rate cases is also visualized in Figure 21. While in both cases, the flow speed at wall are near zero, in the low feed rate case, the flow speed at the center of the tube appears to "speed-up", as the profile of blue color section become "spike-like" shape (20 to 45 s of Figure 21(a)) before entering the conical nozzle. In contrast, in the high feed rate cases, the profile of the blue color section appears to retain "parabolic" shape (5 to 11 s of Figure 21(a)) until entering the conical nozzle. The different appearances of the flows suggested that the flow developments are in different stages. As filament is fed into the heated tube in low feed rate, finite length of filament took longer time to travel the full length of tube than in the high feed rate case. During the long travel time in low feed rate case, more energy is absorbed into the flow, resulting in higher average temperature of flow compared to the high feed rate case. Interface temperature measurement in terms of feed rate shown in section 3.3.1, verified the temperature – feed rate relation. The interface temperature may be used as an indicator of the average temperature of the flow, the higher interface temperature suggests higher average temperature of the flow. With the increase in temperature, both storage modulus [44] and viscosity [9] decreases. The polymer is "fluid-like" in high average temperature and more "solid-like" in low average

temperature. However, direct temperature measurement of the flow in radial direction is difficult. Hence, a numerical tool is used to obtain flow profile and temperature distributions of the extrusion process (section 4.6).

During high feed rate extrusion, small recirculation region measured around 1 – 2 mm can be observed at the top of the gap-filling level, an example is shown in Figure 21(b). The difference color of the recirculating fluid suggests that the polymer flow inside this region is not fixing with the incoming solid filament. Although the recirculation is form by the drag flow generated by downward moving solid filament. The recirculation region is reported in prior publications [11, 12, 30].

### *4.5.2. Kinematic Measurement of Polymer Flow Speed from Video*

From the shown polymer flow development in section 4.5.1, flow velocity magnitude can be obtained through video image analysis. Figure 22 provides an example of making kinematic measurements of the flow speed along the centerline of the tube from the steady extrusion case of $T_e$ = 230 °C and $U$ = 0.5 mm/s.

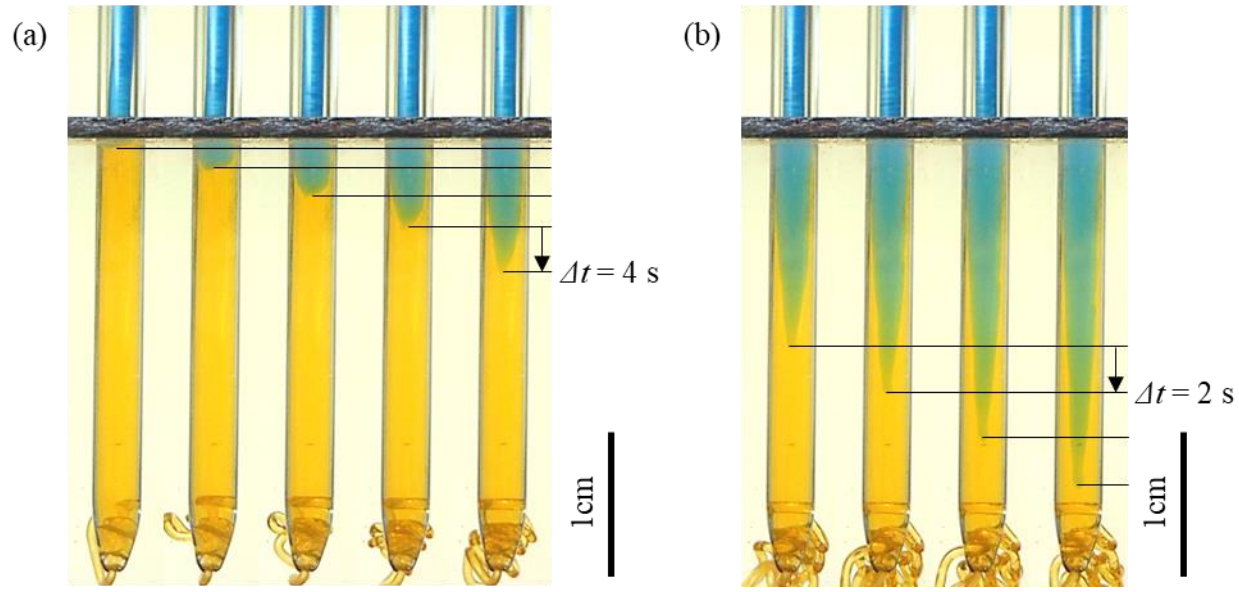


*Figure 22. Example of kinematic measurements of the flow speed along the centerline of the tube of ABS steady extrusion case at $T_e$ = 230 °C and U = 0.5 mm/s (a) developing flow, and (b) developed flow. The time interval Δt between each stroboscopic photo for (a) and (b) are 4 s and 2 s, respectively.*

The interval of time, $\Delta t$ is marked in the stroboscopic photos of the flow displacement profile in Figure 22. While Figure 22(a) shows the flow development after the blue section filament entered the heated section of tube; Figure 22(b) shows the blue section of flow travel in the lower end of the straight tube section. From these stroboscopic photos we can obtain the average flow speed magnitude between two consecutive stroboscopic photos by differentiating the distance travel with respect to time.

As mentioned previously in section 3.2.5, the cylindrical glass tube distorts the image in radial direction except at the center of the tube. This phenomenon makes obtaining the full flow displacement profile in terms of the radius of tube rather complex and inaccurate. For this reason, flow speed magnitude quantitative comparison between the in-situ observed and the simulated are

only carried out along the center line of the tube, while the full flow velocity profile comparison between experimental and numerical results are qualitatively discussed.

## 4.6. Numerical Simulation of Steady Extrusion Process in Heated Tube

Presented in section 4.5, the in-situ experiment revealed the flow development inside heated glass tube during steady extrusion. In this section, examples of simulated extrusion are presented and compared to the experimental measured one. For each set of results, flow profile and temperature distribution are presented at three sampling locations: *I*, *II*, and *III*, which measured 1, 3, and 23 mm from flow entrance, respectively, which are selected for result demonstration (Figure 23).

Locations I and II at near the tube entrance are to capture the flow development when just entering the tube, while the location III is to show the flow development at near the end of the straight section of the tube. At location III, the simulated flow speed magnitude at the center of tube is directly compared to those obtained from the observations.

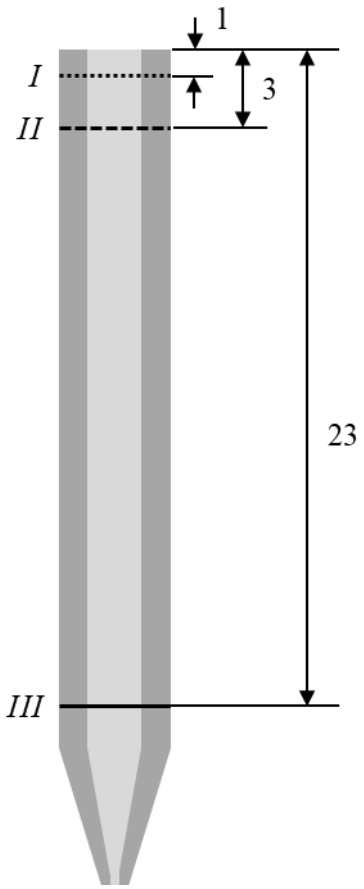


*Figure 23. Flow profile and temperature distribution sampling locations. Location I (dotted line), II (dashed line), and III (solid line) is measured 1, 3, and 23 mm from the entrance, respectively.*

### *4.6.1. Polymer Flow Development in Glass Tube*

The simulated results of the two presented examples in section 4.5 are plotted in Figure 24 and Figure 25, for low (Figure 21 (a)) and high (Figure 21 (b)) feed rate extrusion cases, respectively. For the presented cases, both the viscosity ((a) of Figure 24 and Figure 25) and flow speed magnitude ((b) of Figure 24 and Figure 25) and the polymer flow are plotted against temperature distribution in terms of radius.

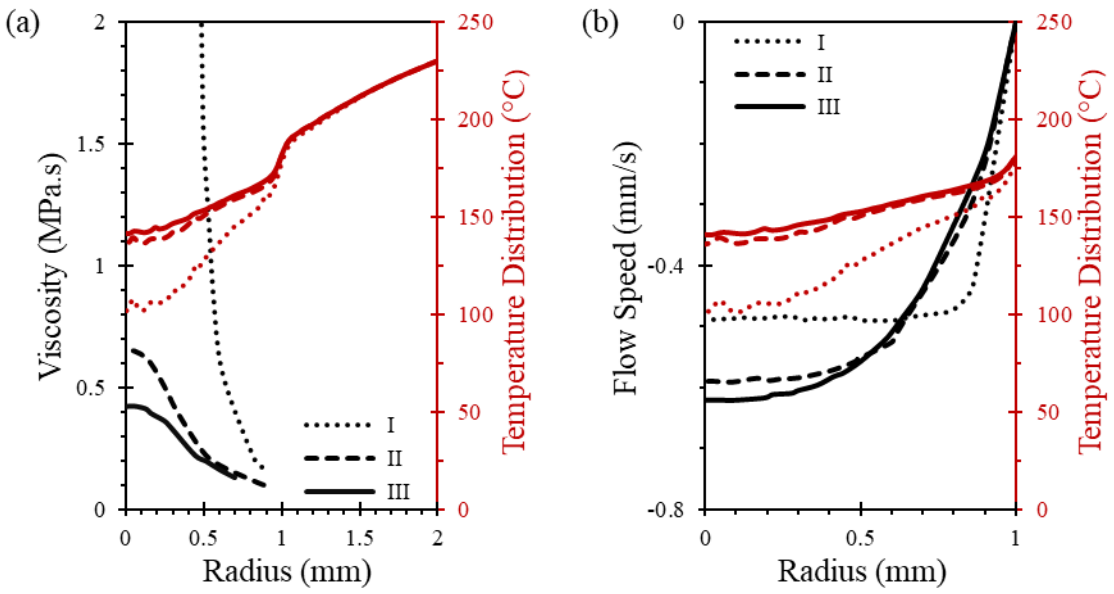


*Figure 24. Simulated low feed rate steady extrusion of ABS in glass tube: $T_e$ = 230 °C and U = 0.5 mm/s. (a) Viscosity; and (b) Flow Speed, against the temperature distribution (Red).*

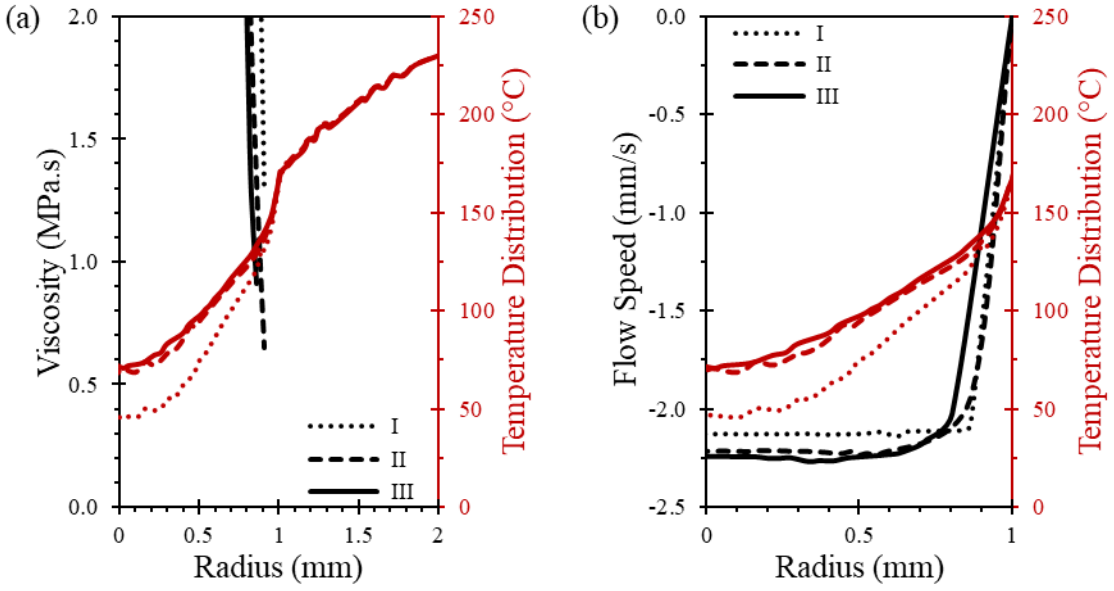


*Figure 25. Simulated high feed rate steady extrusion of ABS in glass tube: $T_e$ = 230 °C and U = 2.5 mm/s. (a) Viscosity; and (b) Flow Speed, against the temperature distribution (Red).*

Note that the 0 radius marks the centerline of the tube; the polymer flow is in between 0 mm and 1 mm radius; and the tube interior is between 1 mm and 2 mm radius. The numerical results are sampled from location *I*, *II*, and *III*. Together, they captured the flow development in the heated tube during steady extrusion.

Temperature distributions exists in both the tube interior and in the polymer flow. The temperature distributions within the glass tube interior are due to the thermal properties of the glass. These differences in temperature distribution are addressed in section 4.6.3 in comparison to aluminum tube quantitatively. For each of the two demonstrated extrusion in glass tube cases, the temperature distributions in the tube interior are nearly identical at the three sampling locations. This suggested the heat flow across the interior of the tube along the length direction of the tube is uniform in each of the shown cases. The temperature drop across the glass tube interior is around 44 °C and 61 °C for the low (Figure 24(a)) and the high (Figure 25(a)) feed rate extrusion cases, respectively. The interface temperature is around 186 °C (Figure 24(b)) and 169 °C (Figure 25(b)) of the respected low and high feed rate cases. The interface temperature is high in the low feed rate case, and it is low in the high feed rate case. This interface temperature trend agreed with the trend of the measured interface temperature measurement shown in section 3.3.1. In the polymer flow of both low and high feed rate cases, the temperature difference in radial direction is larger between locations *I* and *II* than the difference between locations *II* and *III*. Throughout the flow development, the average temperature of the flow at each sampling location is higher in the low feed rate case (Figure 24(b)) than in the high feed rate case (Figure 25(b)), which indicated higher total heat absorption in the low feed rate case.

The viscosity ((a) of Figure 24 and Figure 25) and the velocity profile ((b) of Figure 24 and Figure 25) provided an insight into the conditions of the polymer flow. In the low feed rate case,

the viscosity of the flow decreases from wall towards center of the flow and from location *I* towards location *III*. The viscosity of the flow is correlated to the temperature distribution decreases to below 0.5 MPa.s when reaching location *III* (Figure 24(a)), while the velocity profile turned into a parabolic shape (Figure 24(b)). The parabolic velocity profile indicated the polymer flow is developed. The polymer flow viscosity in the high feed rate case decreased little at near the tube wall, while the center portion are all above 2 MPa.s (Figure 25(a)). The change in associated velocity profile is also minor. The flow velocity at the center of the flow remained uniform when reaching location *III*, which indicated a developing flow (Figure 25(b)). The flow profile comparison in terms of feed rate suggested that the stage of polymer flow development is feed rate dependent. In the low feed rate case, the polymer flow is developed feed rate; while in higher feed rate case, the polymer flow may still be in the developing stage when reaching the end of the straight section of tube.

### *4.6.2. Comparison of Simulated and Measured Speed*

The simulated polymer flows are then compared to the experimental observations (Figure 26). Specifically, we focus our attention on the end of the straight section of the tube (location *III*) at the center of the tube for the flow speed comparison between the simulated and observed cases.

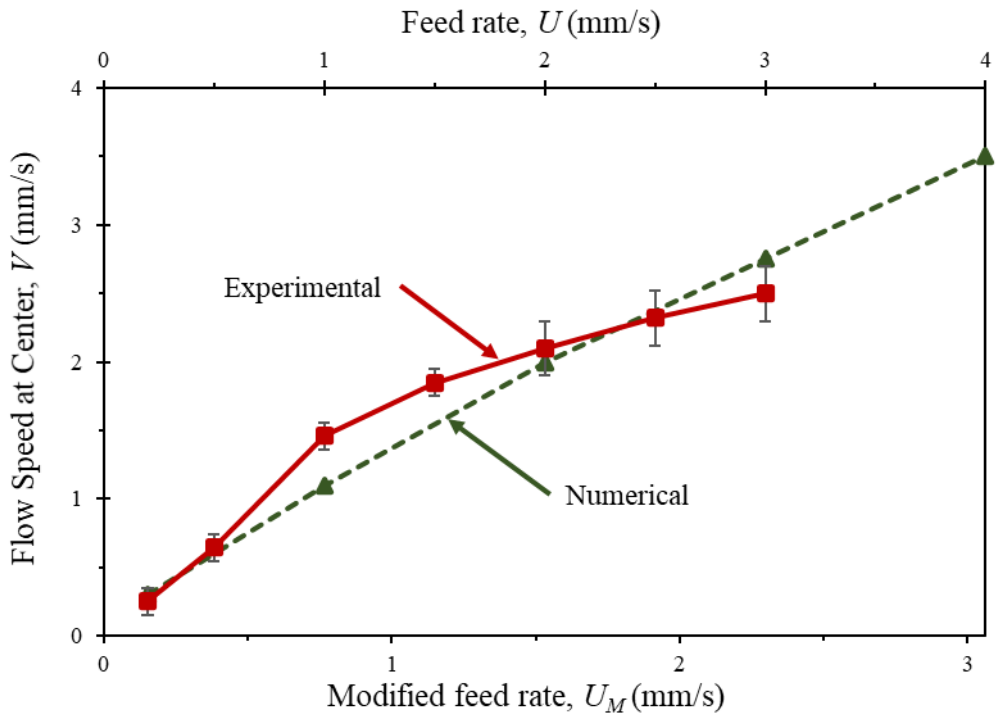


*Figure 26. Simulated flow speed at the center of tube compared to the experimental measurement. Steady extrusion of ABS at $T_e$ = 230 °C, in terms of both feed rate U and modified feed rate $U_M$.*

For the observed cases, the kinematic measurements of flow speed are carried out using the method stated in section 4.5.2. Figure 26 shows the flow speed comparison of extruding ABS at $T_e$ = 230 °C in glass tube. The feed rate above $U$ = 3 mm/s is rarely used in normal printing practice, since extrusion at such high feed rate is unstable, as suggested in several publications [12, 16, 41], the comparisons are carried out up to $U$ = 3 mm/s. The comparisons show good agreement between the simulated speed and the measured speeds (Figure 26). However, noticeable flow speed discrepancy exists between feed rate range of $U$ = 1.0 and 1.5 mm/s. The probable cause contribute to this discrepancy may be the different gap-filling level during steady extrusion. As discussed in section 4.1.1 and section 4.5.2, the gap-filling level varies with feed rate at set extrusion temperature. The gap-filling level is higher in low feed rate cases, as such, the effective

heated length is longer than the length of tube. This gap-filling level in terms of feed rate phenomenon also explains the numerical model over predicted flow speed at feed rate above $U$ = 3 mm/s.

*4.6.3. Polymer Flow Development in Aluminum Tube*

To quantitatively determine the difference extruding ABS filament in different tube material, the ABS extrusions are simulated in aluminum tube with the same boundary conditions. Figure 27 and Figure 28 show the viscosity and flow speed with the respected temperature at the same sampling location *I*, *II*, and *III*.

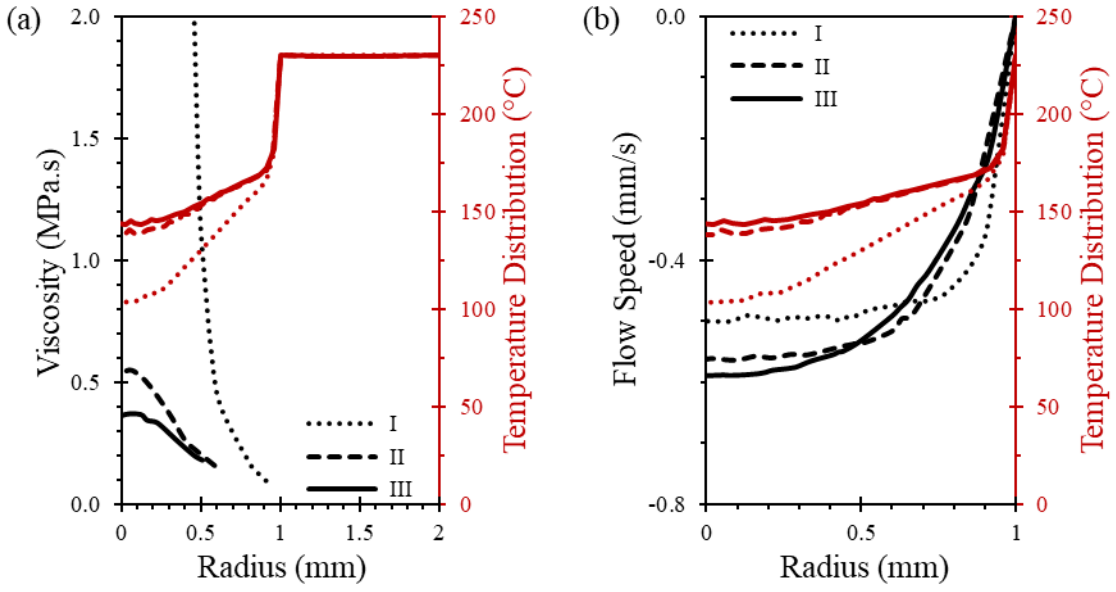


*Figure 27. Simulated low feed rate steady extrusion of ABS in aluminum tube: $T_e$ = 230 °C and U = 0.5 mm/s. (a) Viscosity; and (b) Flow Speed, against the temperature distribution (Red).*

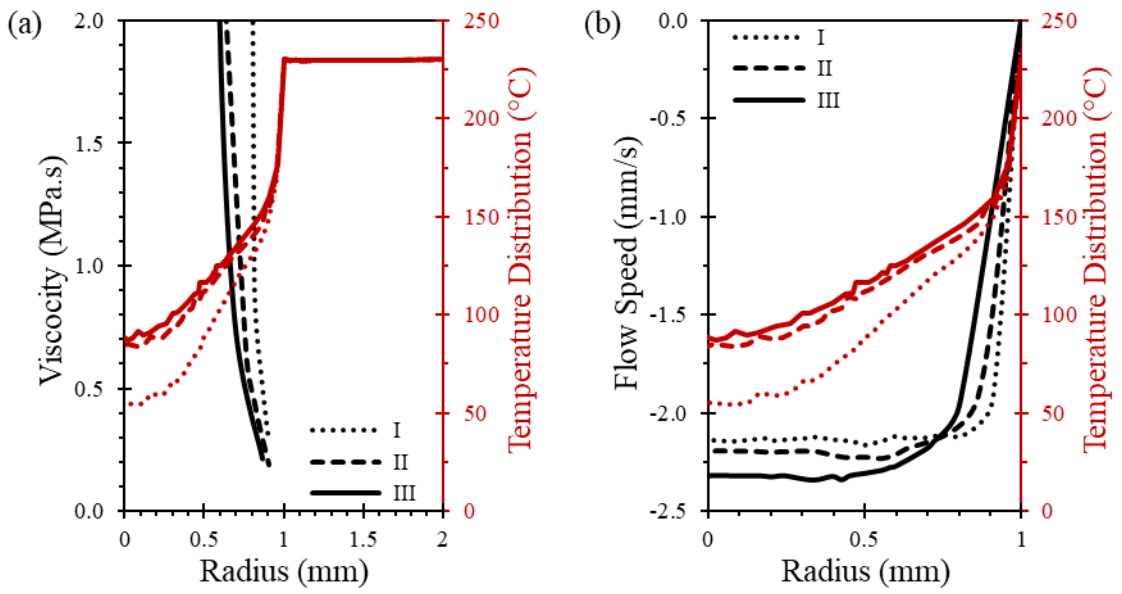


*Figure 28. Simulated high feed rate steady extrusion of ABS in aluminum tube: $T_e$ = 230 °C and U = 2.5 mm/s. (a) Viscosity; and (b) Flow Speed, against the temperature distribution (Red).*

Different from the extrusion case in glass tube, the temperature distribution in the aluminum tube interior stays constant, same as the set temperature of the outer surface. For both two demonstrated aluminum tube extrusion cases (Figure 27 and Figure 28), the temperature throughout the tube interior is 230 °C. The constant temperature distribution in aluminum tube((a) of Figure 27and Figure 28) is due to the 2-order-higher thermal diffusivity of aluminum in comparison to borosilicate glass (

*Table 3*). For high thermal diffusivity material such as aluminum, the thermal inertia is low, the heat can move faster within the material. Hence, the constant temperature distribution within aluminum tube interior. It is for this reason the inner wall temperature of the tube is the same as the set temperature. Different from the glass tube extrusion cases, at all three sampling locations, there are abrupt temperature differences existing in the polymer flow at within 0.1 mm from tube inner walls, which make determining interface temperature rather difficult. Such that,

we consider the temperature at 0.1 mm way from tube's inner wall as the 'interface temperature'. To be specific, that temperature is 172 °C and 159 °C for the low (Figure 27(b)) and the high (Figure 28(b)), respectively. From a comparative view of the polymer flow temperature distribution at the three sampling locations, the polymer flow development outside of the near wall region is similar to those demonstrated glass extrusion cases (Figure 24(b) and Figure 25(b)).

Despite the abrupt temperature difference at near wall region in the aluminum tube extrusion cases, the viscosity ((a) of Figure 27 and Figure 28) and the velocity profile ((b) of Figure 27 and Figure 28) appear similar to those in the glass tube extrusion cases, qualitatively. The polymer flow is developed before reaching the end of the straight section of the tube; while in the high feed rate case, the polymer flow is still developing when reaching the same location.

### *4.6.4. Comparison of Extrusion Processes in Glass and Aluminum Tubes*

We then compare the characteristics of polymer flow of extrusion in both glass and aluminum tubes. The example of flow characteristics comparison is sampled at the end of the straight section of the tube (location *III*). Shown in Figure 29 and Figure 30 are the respected low and high feed rate cases.

In the low feed rate case (Figure 29), the temperature distributions within polymer flow are closely matched till near the tube inner wall. The associated viscosity (Figure 29(a)) and velocity profile (Figure 29(b)) are also closely matched. The similar flow characteristics suggest that in the low feed rate extrusion case, both glass tube and aluminum tube supply abundant amount of heat for melting the filament inside. The melting of filament is limited by the material properties (Table 4) of the filament itself.

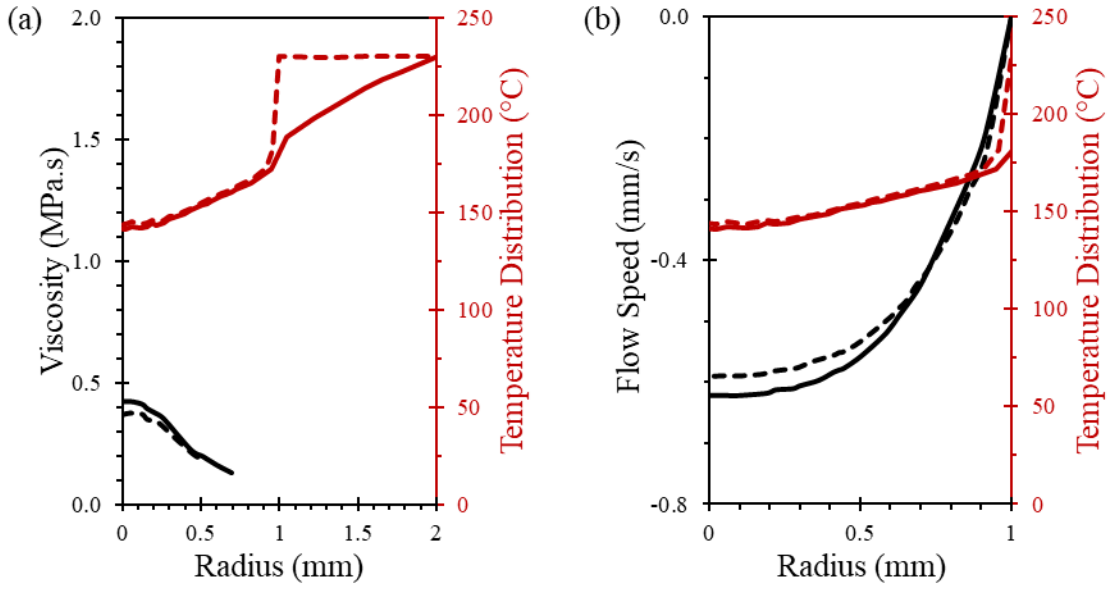


*Figure 29. Comparison of simulated low feed rate steady extrusion of ABS in glass (solid red line) vs. in aluminum (green dashed line) tubes at Location III: $T_e$ = 230 °C and U = 0.5 mm/s. (a) Viscosity; and (b) Flow Speed, against the temperature distribution (Red).*

However, in the high feed rate case (Figure 30), the polymer flow temperature distribution in glass tube is lower than in the aluminum tube cases. The temperature difference between the two temperature distributions is around 20 °C in the center region (exclude the near wall region) of the flows. The lower flow temperature in such cases suggests that the heat supply through glass tube wall is limited due to the comparable inferior thermal properties of glass to aluminum. The lower flow temperature results in higher local viscosity (Figure 30(a)) in glass tube extrusion cases than in the aluminum tube case. And the velocity profiles in Figure 30(b) shows that the profile in glass tube case is in an earlier stage of development than in the aluminum tube case. However, the difference in velocity profile is relatively small in the presented cases.

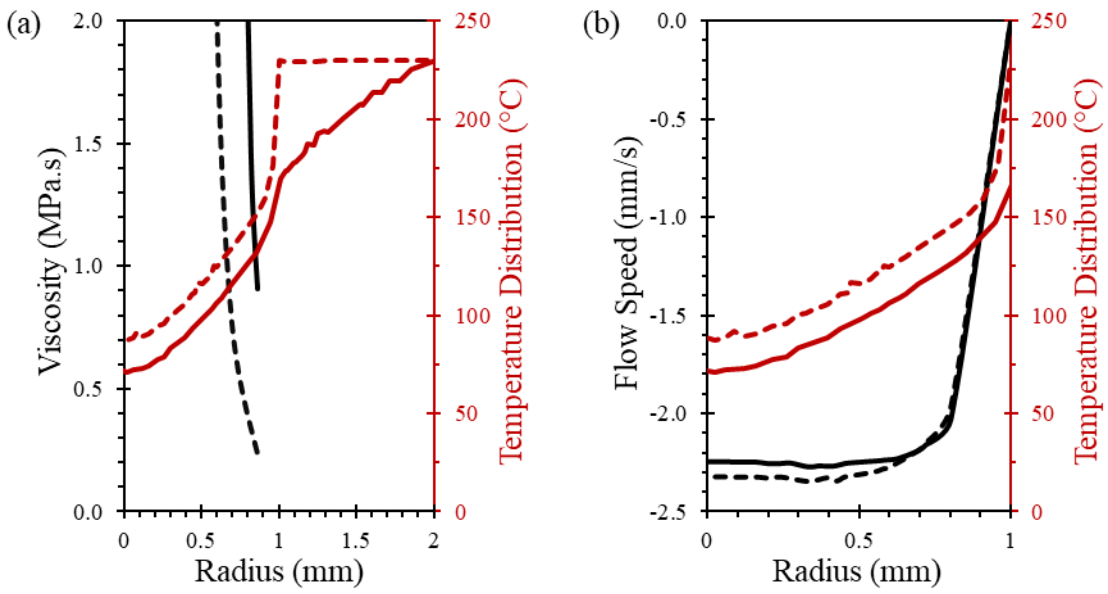


*Figure 30. Comparison of simulated high feed rate steady extrusion of ABS in glass (solid red line) vs. in aluminum (green dashed line) tubes at Location III: $T_e$ = 230 °C and $U$ = 2.5 mm/s. (a) Viscosity; and (b) Flow Speed, against the temperature distribution (Red).*

In all, from the above comparisons (Figure 29 and Figure 30), two points are concluded: i) with abundant heat supply, such as low feed rate extrusion cases in glass tube (Figure 24), as well as both low and high feed rate extrusion cases in aluminum tube (Figure 27 and Figure 28), the heating of polymer in such condition is polymeric thermal properties dependent , specifically the low thermal diffusivity (Table 4) of ABS; and ii) with limited heat supply, such as high feed rate extrusion in glass tube cases (Figure 25), the heating of polymer is heat supply dependent. Further increasing filament feed rate in glass tube cases at a set extrusion temperature, the polymer extrusion process would enter the 'clogging' region, as discussed in section 4.2. For glass tube ABS extrusion cases at extrusion temperature of $T_e$ = 230 °C, the experimental determined critical feed rate is $U$ = 4.05 mm/s (Figure 15). When provided with sufficiently high feed rate, the aluminum tube case can also become heat supply dependent, and polymer extrusion become

‘unstable’. This critical feed rate, or upper bound feed rate can be determined by using the method presented in Luo et al. [16].

# CHAPTER 5

# CONCLUSION

## 5.1. Summary of Work

In this work, we explore the polymer extrusion process in MatEx via experimental and numerical investigations, to address the extrusion process in material extrusion additive manufacturing. In the experimental part of this work, we design and build an experimental apparatus to directly observe the extrusion processes of ABS and PLA. The in-situ observation reveals the three-step gap-filling model of the extrusion process. Then, the transient extrusion processes of changing filament and resume extrusion are observed and qualitatively discussed.

The steady extrusion is investigated through combined experimental and numerical investigations. The numerical work is conducted based on the experimental setup with ABS only. Two sets of numerical work are conducted in the same boundary conditions: one set is simulated with glass tube, and other set is with aluminum tube. In the case of glass tube, the simulated polymer flow speed is compared to the experimental observed counterpart. Then, the polymer flow profiles in both the cases of glass and aluminum tubes are compared for the purposes of validating the performance of the built apparatus and expanding the scope of this work.

## 5.2. Concluding points

In all, there are four concluding points from the in-situ observation of the polymer extrusion processes in additive manufacturing:

1) When the gap between the inner surface of the glass tube and the edge of the filament is filled, the image of the filament appears to penetrate the tube wall. This phenomenon can be used to judge whether a gap is filled.
2) As the filament has a slightly curved shape, the edge of its front has direct contact with the tube wall. The gap-filling starts at this edge once the temperature of the polymer in the neighborhood of this edge reaches $T_c$. During the gap-filling process, the solid core of the filament functions as a plunger to drive the surrounding polymer melt against the tube wall. The polymer melt may spread both upwards and downwards on the tube wall. When the filament front gets into the conical nozzle of the tube, the driving force is increased, causing the further rise of the gap-filling level. The final filling level remains almost unchanged when the extrusion reaches steady state. Due to the similarity in the extruder, the observed gap-filling process may apply to the case of a MatEx 3D printer, as validated using a commercial extruder.
3) Depending on the feed rate and extrusion temperature, a heated tube may be over- or partial-filled during stead-state extrusion for both materials. Since at least 90% of the heated tube is fully filled in a partially-filled case, it appears reasonable to assume the tube is fully filled in modelling the temperature and pressure distribution, as done in the existing thermal or pressure models [13, 14, 15, 16, 17].
4) The gap-filling level during a steady-state extrusion does not depend on how the extrusion starts. It may start with an empty or pre-filled extruder. As air bubbles may be involved in

initial extrusion, it is recommended that the printing starts after the filament has run through the extruder a couple of times.

The simulation model and boundary conditions were selected based on the in-situ observation of the steady extrusion process. The simulation model and boundary conditions were validated by comparing the simulated flow profile with the in-situ observed result. By comparing the polymer flow characteristics from the cases of extrusion processes in glass and the aluminum tubes, i) polymer is sufficiently heated in the cases of low feed rates, the flow characteristics are similar in the cases of glass and aluminum tubes; ii) polymer is insufficiently heated in high feed rate cases, mainly due to short heating time, as well as the low thermal diffusivity of the polymeric material; and iii) as heat transfers faster through the aluminum tube to the polymer, the feed rate that causes clogging in the case of aluminum tube is higher than its counterpart in the case of the glass tube.

## 5.3. Future Work

This work experimentally investigated gap-filling processes and provided possible explanation of the phenomena during different extrusion scenarios for both ABS and PLA filaments. The numerical model revealed the flow characteristics in the glass tube as well as in the aluminum tube. The latter is often used in a conventional MatEx extruder.

To our knowledge, this in-situ observation is a novel approach of revealing the flow characteristics of polymer extrusion process for MatEx based additive manufacturing. Naturally,

there are many areas that can be improved in the future work. Some potential developments are indicated below:

1) The glass tube may be further incorporated into a conventional printer. Consequently, the corresponding extrudates could be used to form printed parts. This would make it possible to link the polymer behavior observed inside the glass tube with the quality of the printed parts.
2) The current experiment explored the extrusion process of two commonly used filament type by visualization. The flow characteristics of composite polymers, such as carbon-fiber filled filament and filaments with added foaming agents, would be interesting to explore in the future.
3) The finding of this work provided insights on optimizing the extruder hot-end geometries for high-speed extrusion purpose.

# APPENDIX I

## FILAMENT FEED RATE CONTROL & CALIBRATION

The feed rate is calibrated with the feed gear in the extruder motor and the HATCHBOX filament (1.75mm diameter). The calibration is carried out by measuring the feed rate in terms of interval. The feed rate vs interval is then plotted inversely and fitted with Equation (A-1):

$$Interval = 2529.5{U_f}^{-1.011} \quad \text{(A-1)}$$

The calibration curve is plotted in Figure 31. The sample feed rate control program as attached below. To change feed rate, replace the number in the Interval in the attached code with the 'interval' number with the respective filament feed rate from Figure 31.

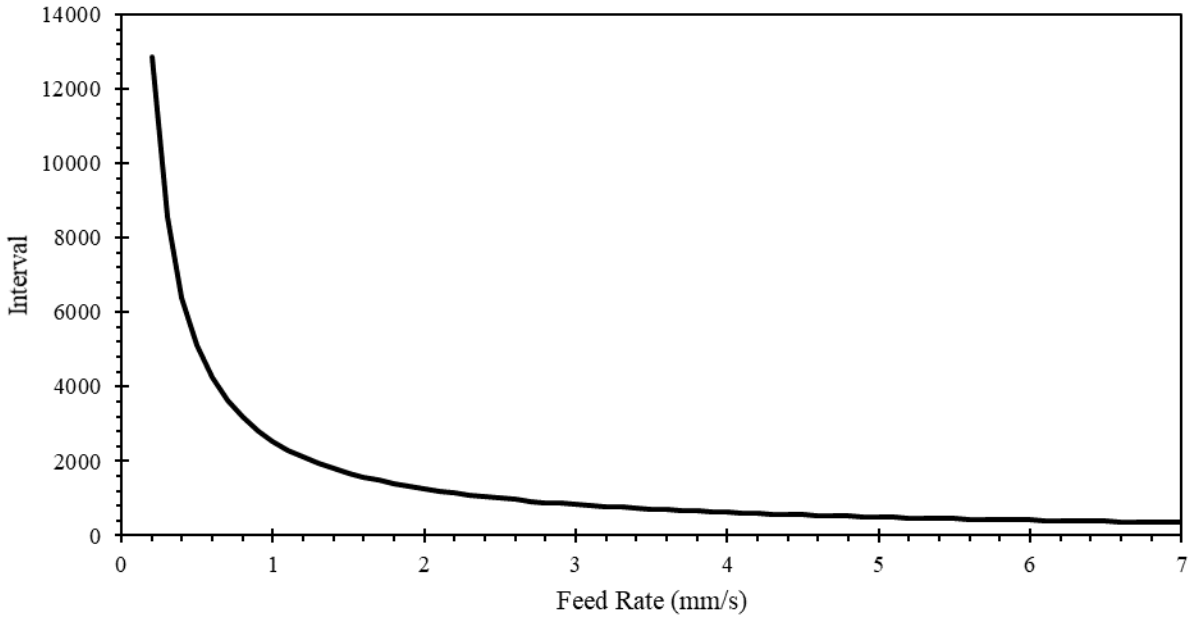


*Figure 31. Filament feed rate calibration curve*

Feed rate control code

```
const int Ena = 2; // Enable
const int Dir = 3; // Direction
const int Pul = 4; // Take one step
const int Interval = 2529.5; // Interval = 2529.5*Vfi^-1.011
boolean Pulse = LOW; // Changes in Pulse State
void setup()
{
  pinMode(Ena, OUTPUT);
  pinMode(Dir, OUTPUT);
  pinMode(Pul, OUTPUT);
  digitalWrite(Ena, LOW);  // Enable Inverted - LOW
  digitalWrite(Dir, LOW);  // CW - LOW / CCW - HIGH
  digitalWrite(Pul, HIGH); // Downhill Edge
}
void loop()
{
  Pulse = !Pulse; //Inverts the State of the Variable
  digitalWrite(Pul, Pulse); //Assign the new state to the port
  delayMicroseconds(Interval);
}
```

# APPENDIX II

## TEMPERATURE MEASUREMENT

The temperature measurements are taken using K-Type thermocouples (OMEGA Engineering, Norwalk, CT, USA) with data acquisition (DAQ) hardware (National Instrument 9212 C series, Austin, TX, USA). The temperature monitoring and recording are taken using LabVIEW, virtual programing language developed by National Instruments (Austin, TX, USA). Figure 32 and Figure 33 shows the block diagram and front panel of the temperature monitoring recording DAQ, respectively.

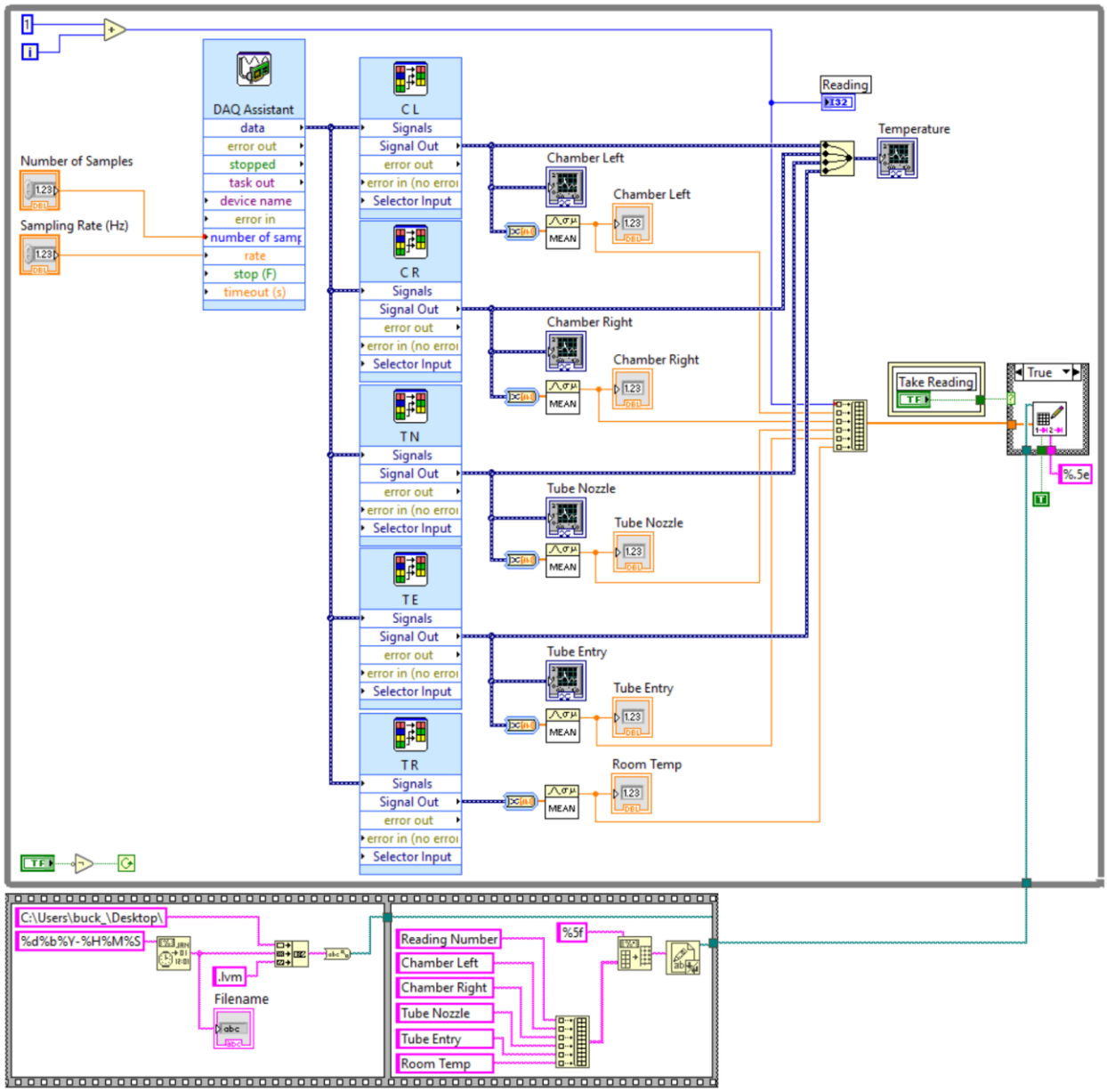


*Figure 32. LabVIEW block diagram for temperature monitoring and recording*

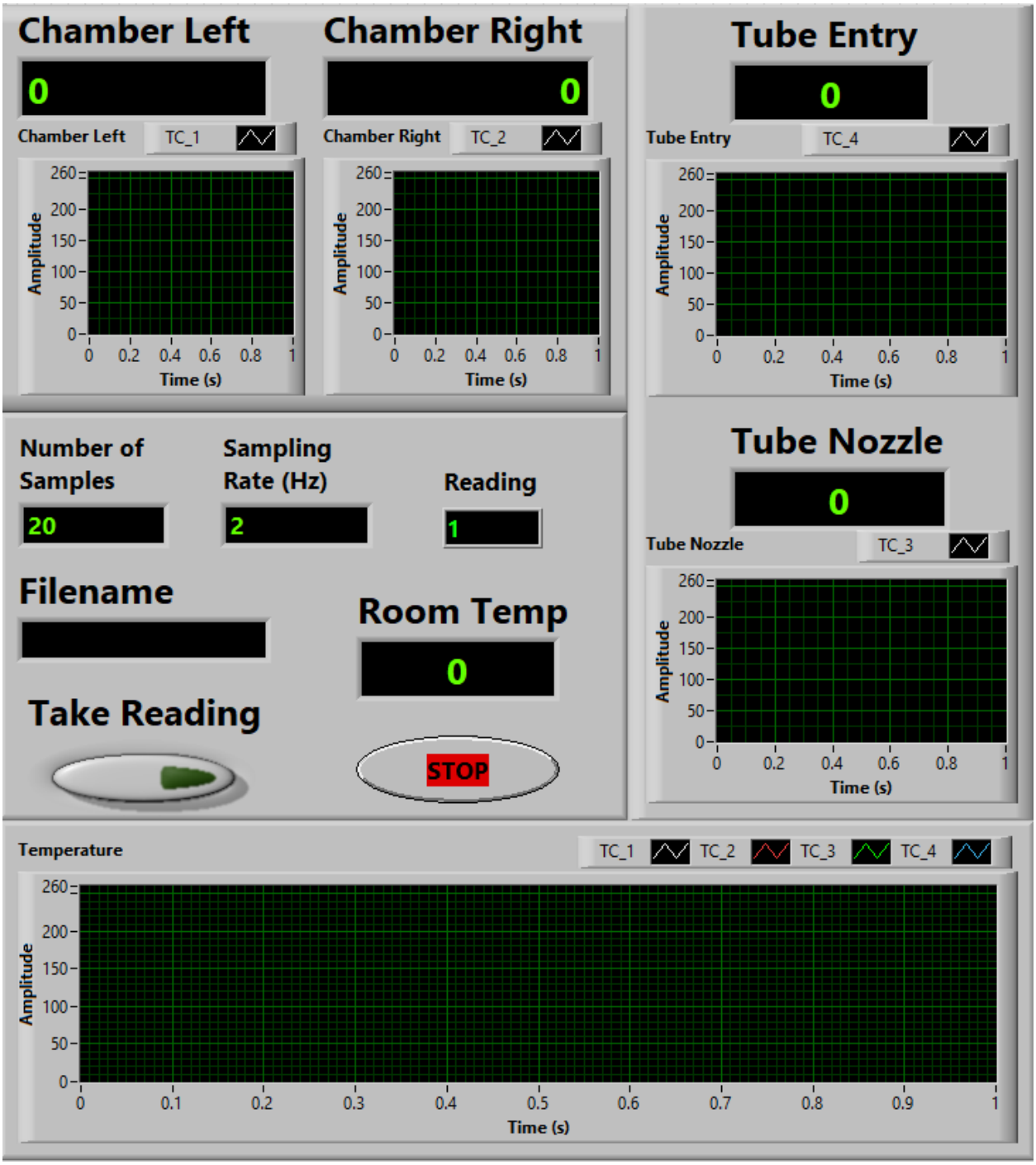


*Figure 33. LabVIEW front panel for temperature monitoring and recording*

# APPENDIX III

## LIGHT DEFLECTION IN CYLINDRICAL TUBE

Figure 34(b) gives top-down illustrations of one ray path through glass cylinder. In Figure 34(b) left, supposed an incident ray tangent to the point $P$ travel inside the glass wall from $P$ to $Q_1$, form the angle of incident $\alpha$ to the normal of the tube outer surface. The light then refracted into air towards $Q_2$, the refracted angle is $\alpha'$ to the normal of the tube outer surface. If the observer's view is parallel the center line $OO'$, the point $P$ is at the location of $P'$. In other words, the true inner wall radius $r_i$ is magnified to its observed radius $r_i'$. Figure 34(b) right show a similar story only the tube is filled with filament. These two cases shown that when filament's image radius is equal to the radius of the image of inner wall ink residue, the filament is in contact with the tube inner wall. Note that, conveniently, this optical distortion appears to only shows well when the filament insert is in large enough contact with the tube wall, similar to the one shown in Figure 34(a) right; if the contact area is limited such as Figure 34(a) left, the contact area would be hard to detect.

The optical distortion of the filament is also an indicator of the filament is deformed in sufficiently large volume. A quasi-steady state heated transfer experiment is also conducted to determine the lowest critical temperature for filament fully filled the cross section of tube with our setup. When filament is fed into the heated tube at a low feed rate of $U_f$ = 0.2 mm/s, this critical temperature is found at $T_c$ = 125 °C, which is higher than the glass transitional temperature of $T_g$ = 105 °C [9]. At above $T_c$, the storage modulus of ABS drops exponentially compared to at $T_g$, the filament's ability to store the mechanical energy in terms of feed force become much less, the

heated filament become appliable. In other words, in an ideal setting of large finite feed force and infinitely small feed rate, for amorphous polymer such as ABS, we should expect the critical temperature, $T_c$ infinitely approach glass transitional temperature $T_g$ [9].

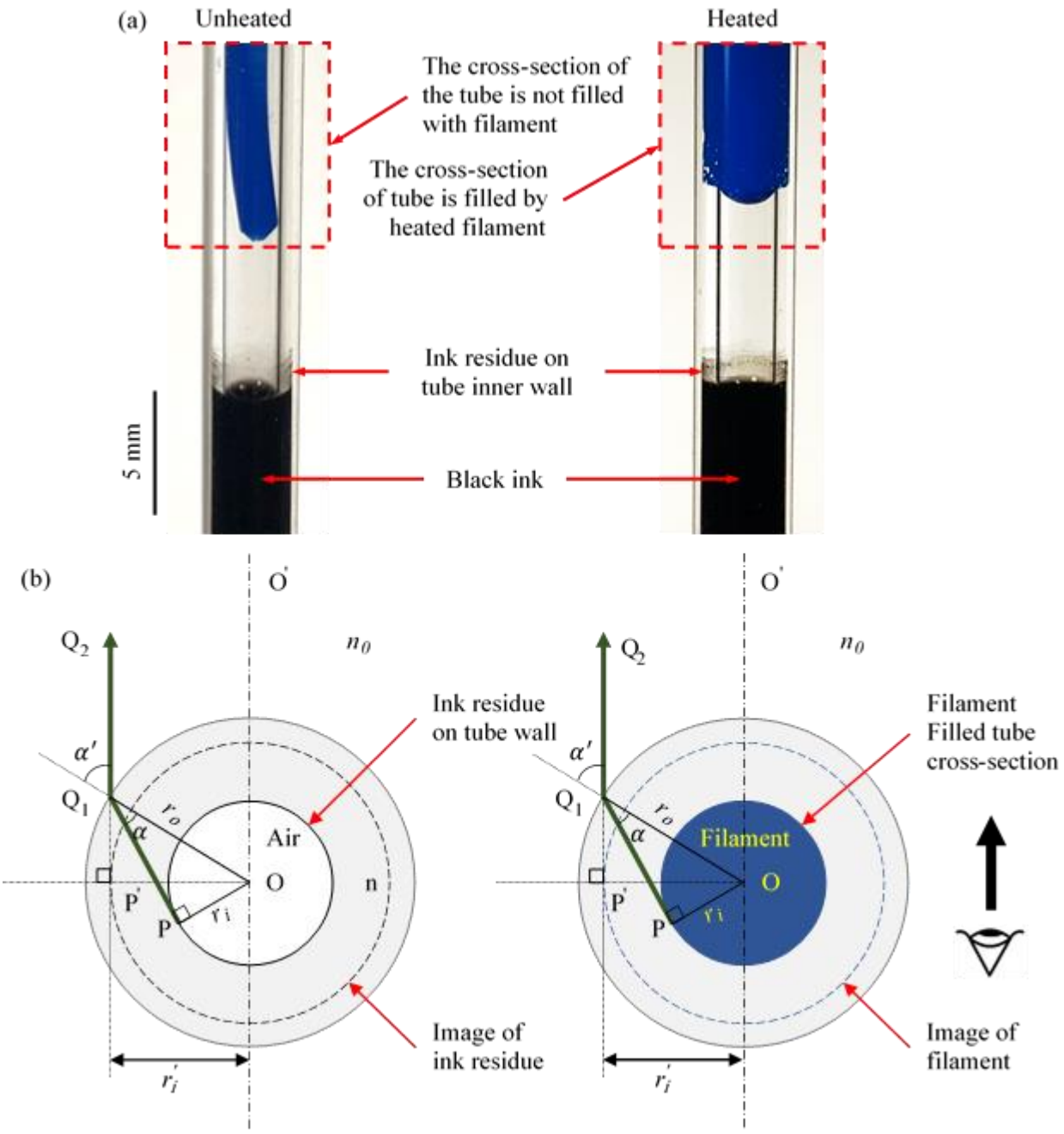


*Figure 34. Light deflection in cylindrical tube. (a) A comparative view between solid filament and melted filament inserted in tube: left shows filament in room temperature inserted in glass tube, right shows heated filament filled cross-section of the tube; (b) A top-down illustration of one ray path in green according to Snell's Law*

# REFERENCE


[1] H. Kodama, "Stereoscopic figure drawing device". Japan Patent JPS56144478A, 1980.

[2] H. Kodama, "Automatic method for fabricating a three-dimensional plastic model with photo-hardening polymer," *Review of Scientific Instruments,* vol. 52, p. 1770, 1981.

[3] A. L. Méhauté, O. d. Witte and a. J. C. André, "Dispositif pour realiser un modele de piece industrielle". France Patent FR2567668, 1984.

[4] C. W. Hull, "Apparatus for production of three-dimensional objects by stereolithography". USA Patent US4575330A, 1984.

[5] C. R. Deckard, "Method and apparatus for producing parts by selective sintering". USA Patent US4863538A, 1986.

[6] W. Meiners, K. D. Wissenbach and A. D. Gasser, "Verfahren zur Herstellung eines Formkörpers". Germany Patent DE19649865C1, 1996.

[7] S. S. Crump, "Apparatus and method for creating three-dimensional objects". USA Patent US5121329A, 1989.

[8] B. N. Turner, R. Strong and S. A. Gold, "A review of melt extrusion additive manufacturing processes: I. Process design and modeling," *Rapid Prototyping Journal,* vol. 20, no. 3, pp. 192 - 204, 2014.

[9] J. E. Seppala, S. H. Han, K. E. Hillgartner, C. S. Davis and K. B. Miglera, "Weld formation during material extrusion additive manufacturing," *Soft Matter,* vol. 13, pp. 6761 - 6769, 2017.

[10] E. L. Gilmer, D. Miller, C. A. Chatham, C. Zawaski, J. J. Fallon, A. Pekkanen, T. E. Long, C. B. Williams and M. J. Bortner, "Model analysis of feedstock behavior in fused filament fabrication: Enabling rapid materials screening," *Polymer,* vol. 152, pp. 51 - 61, 2018.

[11] M. E. Mackay, "The importance of rheological behavior in the additive manufacturing technique material extrusion," *Journal of Rheology,* vol. 62, p. 1549, 2018.

[12] M. P. Serdeczny, R. Comminal, M. T. Mollah and D. B. Pedersen, "Numerical modeling of the polymer flow through the hot-end in filament-based material extrusion additive manufacturing," *Additive Manufacturing,* vol. 36, p. 101454, 2020.

[13] A. Bellini, S. Gu¨c¸er and M. Bertoldi, "Liquefier dynamics in fused deposition," *Journal of Manufacturing Science and Engineering,* vol. 126, pp. 237 - 246, 2004.

[14] M. E. Mackay, Z. R. Swain, C. R. Banbury, D. D. Phan and D. A. Edwards, "The performance of the hot end in a plasticating 3D printer," *Journal of Rheology,* vol. 61, pp. 229 - 236, 2017.

[15] D. D. Phan, Z. R. Swain and M. E. Mackay, "Rheological and heat transfer effects in fused filament fabrication," *Journal of Rheology,* vol. 62, pp. 1097 - 1107, 2018.

[16] C. Luo, X. Wang, K. B. Migler and J. E. Seppala, "Upper bound of feed rates in thermoplastic material extrusion additive manufacturing," *Additive Manufacturing,* vol. 32, p. 101019, 2020.

[17] C. Luo, X. Wang, K. B. Migler and J. E. Seppala, "Effects of feed rates on temperature profiles and feed forces in material extrusion additive manufacturing," *Additive Manufacturing,* vol. 35, p. 101361, 2020.

[18] T. B. Drew, "Mathematical attacks on forced convection problems, a review," *Trans. Am. Inst. Chem. Eng. Sci.,* vol. 26, pp. 26 - 80, 1931.

[19] B. C.Lyche and R.ByronBird, "The Graetz-Nusselt problem for a power-law non-newtonian fluid," *Chemical Engineering Science,* vol. 6, no. 1, pp. 35 - 41, 1956.

[20] E. E. Agur and J. Vlachopoulos, "Heat Transfer to Molten Polymer Flow in Tubes," *Journal of Applied Polymer Science,* vol. 26, no. 3, pp. 765 - 773, 1981.

[21] D. Wei and H. Luo, "Finite element solutions of heat transfer in molten," *International Journal of Heat and Mass Transfer,* vol. 46, pp. 3097 - 3108, 2003.

[22] C. Luo, "Determination of constant viscosity for a power-law melt flow inside a circular tube," *Chemical Engineering Science,* vol. 195, pp. 239 - 241, 2019.

[23] R. B. Bird, W. E. Stewart and E. N. Lightfoot, Transport Phenomena 2nd Edition, John Wiley & Sons, Inc., 2002.

[24] R. L. Boles, H. L. Davis and D. C. Bogue, "Entrance Flows of Polymeric Materials: Pressure Drop and Flow Patterns," *Polymer Engineering and Science,* vol. 10, no. 1, pp. 24 - 31, 1970.

[25] M. P. Serdeczny, R. Comminal, D. B. Pedersen and J. Spangenberg, "Experimental and analytical study of the polymer melt flow through the hot-end in material extrusion additive manufacturing," *Additive Manufacturing,* vol. 32, p. 100997, 2020.

[26] S. B. Balani, F. Chabert, V. Nassiet and A. Cantarel, "Influence of printing parameters on the stability of deposited beads in fused filament fabrication of poly(lactic) acid," *Additive Manufacturing,* vol. 25, pp. 112 - 121, 2019.

[27] C. Luo, M. Mrinal, X. Wang and Y. Hong, "Bonding widths of deposited Polymer strands in additive manufacturing," *Materials,* vol. 14, p. 871, 2021.

[28] T. A. Osswald, J. Puentes and J. Kattinger, "Fused filament fabrication melting model," *Additive Manufacturing,* vol. 22, pp. 51 - 59, 2018.

[29] F. Peng, B. D. Vogt and M. Cakmak, "Complex flow and temperature history during melt extrusion in material extrusion additive manufacturing," *Additive Manufacturing,* vol. 22, pp. 197 - 206, 2018.

[30] D. D. Phan, J. S. Horner, Z. R. Swain, A. N. Beris and M. E. Mackay, "Computational fluid dynamics simulation of the melting process in the fused filament fabrication additive manufacturing technique," *Additive Manufacturing,* vol. 33, no. 101161, 2020.

[31] "HATCHBOX ABS 3D Printer Filament," 3 1 2017. [Online]. Available: https://cdn.shopify.com/s/files/1/0008/2457/4018/files/HATCHBOX_ABS_3D_Printer_Filament_SDS.pdf?1561. [Accessed 2022].

[32] "HATCHBOX PLA 3D Printer Filament," 11 1 2016. [Online]. Available: https://cdn.shopify.com/s/files/1/0008/2457/4018/files/HATCHBOX_PLA_3D_Printer_Filament_SDS.pdf?1561. [Accessed 2022].

[33] M. Darzi and C. Park, "Optical distortion correction of a liquid-gas interface and contact angle in cylindrical tubes," *Physics of Fluids,* vol. 29, p. 052004, 2017.

[34] Y.-K. An, "Simple method to measure the refractive index of liquid with graduated cylinder and beaker," *Review of Scientific Instruments,* vol. 88, p. 125105, 2017.

[35] J. Jyoti, B. P. Singh, A. K. Arya and S. R. Dhakate, "Dynamic mechanical properties of multiwall carbon nanotube reinforced ABS composites and their correlation with entanglement density, adhesion, reinforcement and C factor," *RSC Advances,* vol. 6, pp. 3997 - 4006, 2016.

[36] N. Othman, B. Jazrawi, P. Mehrkhodavandi and S. G. Hatzikiriakos, "Wall slip and melt fracture of poly(lactides)," *Rheol Acta,* vol. 51, pp. 357 - 369, 2012.

[37] R. F. Barron and B. R. Barron, Design for Thermal Stresses, John Wiley & Sons, Inc., 2012.

[38] J. Blumm, A. Lindemann, M. Meyer and C. Strasser, "Characterization of PTFE Using Advanced Thermal Analysis Techniques," *International Journal of Thermophyscis,* vol. 31, pp. 1919 - 1927, 2010.

[39] L. F. Johnson, D. P. H. Hasselman and E. Minford, "Thermal diffusivity and conductivity of a carbon fibre-reinforced borosilicate glass," *Journal of Materials Science,* vol. 22, pp. 3111 - 3117, 2987.

[40] "Solving Larger, More Complex Systems Using Ansys 2021 R1," [Online]. Available: https://www.ansys.com/blog/solving-larger-more-complex-systems-2021-r1. [Accessed 2022].

[41] Y. Hong, M. Mrinal, H. S. Phan, V. D. Tran, X. Liu and C. Luo, "In-situ observation of the extrusion processes of Acrylonitrile Butadiene Styrene and Polylactic Acid for material extrusion additive manufacturing," *Additive Manufacturing,* vol. 49, p. 102507, 2022.

[42] "Granta Materials Data for Simulation (MDS)," ANSYS, 2021.

[43] Z. Tadmor and C. Gogos, Principles of Polymer Processing, 2nd Edition, John Wiley & Sons. lnc., 2006.

[44] Z. Weng, J. Wang, T. Senthil and L. Wu, "Mechanical and thermal properties of ABS/montmorillonite nanocomposites for fused deposition modeling 3D printing," *Materials and Design,* vol. 102, pp. 276 - 283, 2016.

[45] B. Coppola, Nicola Cappetti, L. D. Maio, P. Scarfato and L. Incarnato, "3D Printing of PLA/clay Nanocomposites: Influence of Printing Temperature on Printed Samples Properties," *Materials,* vol. 11, p. 1947, 2018.